

# **Part I**

# **Operations**

## **Part II**

# **Installations**

## **Part III**

# **Telescope and Instrument**

# Chapter 15

## The Huitzi $f/20$ Imager

The Huitzi  $f/20$  imager was installed on the COATLI telescope in December 2022. The imager is named for the mexica god **Huītziłōpōchtlī**, the son of the goddess Coatlicue.

Earlier, the “Interim Imager” and “Huitzi  $f/8$  Imager” were installed on the telescope. For historical reference, these are described in Appendices B and ??.

### 15.1 Overview

Figure 15.1 shows the Huitzi  $f/20$  imager on the telescope.

The imager uses a 150 mm diverging lens to convert the  $f/8$  beam of the telescope into an  $f/20$  beam. This beam is then imaged an Andor iXon electron-multiplying CCD detector with  $1024 \times 1024$  pixels with a pixel scale of 0.27 arcsec and a field of 4.6 arcmin. The detector can be read through either a conventional amplifier or the electron-multiplying amplifier at a variety of speeds.

The imager has three Finger Lakes Instruments filter wheels. Currently, the following filters can be provided:

- open: Completely open.
- dark: Completely blocked.
- grizy: Filters similar to the Pan-STARRS equivalents. Note, however, that while the filters are similar, the CCD is not deep-depleted and so the bandpasses are somewhat different.
- w: A filter that combines the  $r$  and  $i$  bands. Note that this is different to Pan-STARRS  $w$  which includes the  $g$  band too. It is mainly intended for sensitive imaging of GRBs.
- BVRI: Johnson-Cousins filters according to the Bessell formulation.
- $I_s$ : The  $I$  filter with a sharp red cutoff at 900 nm. This is intended to better match the bandpass of the original Cousins (1978)  $I$  photometry. The blue edge is the same as the Bessell formulation, but the red edge is defined by a 900 nm short-pass filter to simulate the red edge of a GaAs tube. The Bessell (1990) and Bessell & Murphy (2012) bandpasses fall at about 900 nm.

- 470/10, 515/10, and 640/10: Nebular continuum filters.
- 501/8, 656/3, 656/8: Nebular line filters.

Some of these filters are constructed from combinations of filters in different wheels, as described in more detail below.

The detector is mounted on Optec Gemini focuser and rotator, which allows up to 12.7 mm of motion of the detector with respect to the lens.

### 15.2 Optics

The effect of the negative lens is shown schematically in Figure 15.2.  $A$  is the position of the telescope focus without the lens.  $S$  is the position of the lens.  $A'$  is the position of the telescope focus with the lens. The magnification  $m$  is given by

$$m = SA'/SA,$$

in which  $SA'$  and  $SA$  are optical distances. If the focal length of the lens is  $F$ , then Gauss' equation gives the relation between  $SA$  and  $SA'$  as:

$$1/F = 1/SA' - 1/SA.$$

We then solve to find:

$$m = 1 - SA'/F$$

and

$$SA' = -(m - 1)F.$$

We can see the approximate dimensions of the system by ignoring chromatic aberration and taking  $F = -150$  mm. Then, if we choose  $SA = 90$  mm we have  $SA' = 225$  mm and  $m = 2.5$ . Since the focal ratio of the telescope is  $f/8$ , this magnification gives a focal ratio of  $f/20$ .

The actual lens is Edmund Optics part #63-767, whose design is shown in Figure 15.3. It has a design effective focal length of  $-150$  mm at 587.6 nm. It is nominally 40 mm in diameter and 13.54 mm thick at the edge. The precise optical and mechanical prescriptions are given in the files “zmax\_63767.ZMX” and “step\_63767.STP” supplied by Edmund Optics. The lens is used with the convergent element B uppermost (towards the



Figure 15.1: The Huitzi  $f/20$  imager on the COATLI telescope.

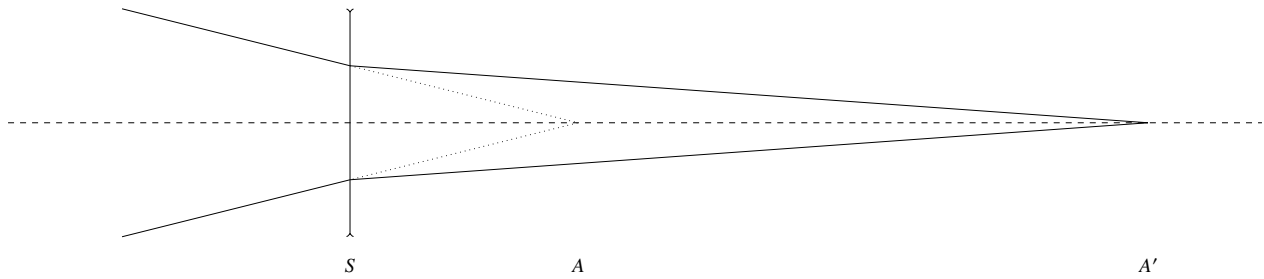


Figure 15.2: Schematic of the Optical Design

secondary) and the divergent element A lowermost (towards the detector). That is, surface S4 is uppermost (towards the secondary) and surface S1 is lowermost (towards the detector). If the lens is inverted, the system will suffer significant spherical aberration.

The lens is an achromatic doublet, so its focal length varies with wavelength. This has two effects. First, the different focal length between bands requires us to refocus for each filter. In theory, we could adjust both the secondary and the focuser to achieve focus while holding the magnification constant. In practice, we simply adjust the focuser to maintain focus and let the magnification vary slightly. (The focuser is also used to compensate for the different optical thicknesses of the filters.) Second, chromatic aberration within the *g* and *B* bands limits their image quality.

The lens has a  $\lambda/4$  MgF<sub>2</sub> coating on both surfaces.

The lens also serves as a window to prevent ingress of dust and insects.

### 15.3 Filters

The upper filter wheel (“A”) is an FLI CFW-1-5 wheel for five 50 mm diameter filters. The two lower filter wheels (“B” and “C”) are FLI CFW-1-8 wheels for eight 25 mm diameter filters. The elements installed in each wheel are shown in Table 15.1.

The filter elements are:

- *griz*: These are similar to the Pan STARRS filters. They were acquired from Custom Scientific and fabricated to our specifications. They are 25 mm in diameter and 5 mm thick. They have dielectric coatings on fused silica substrates.
- *BVRI*: These are Johnson-Cousins filters adapted from the Bessell (1990) recipe. They are off-the-shelf filters acquired from Custom Scientific. They are 50 mm (*BVR*) or 25 mm (*I*) diameter and 5 mm thick. From modeling the transmission curves, we believe the recipes are:
  - *B*: 2 mm Hoya L38 + 1 mm Schott BG25 + 2 mm Schott BG39

- *V*: 1 mm Schott GG495 + 3 mm Schott BG39 + 1 mm filler

- *R*: 2 mm Schott OG570 + 3 mm Schott KG3

- *I*: 3 mm Schott RG9 + 2 mm filler

- 825SP: This is an 825 nm OD4 short-pass filter. It is Edmund Optics part #86-113. It is 50 mm in diameter and 5 mm thick. It has dielectric coatings on a fused silica substrate.
- 925LP: This is an 925 nm OD4 long-pass filter. It is Edmund Optics part #86-072. It is 25 mm in diameter and 3 mm thick. It has dielectric coatings on a fused silica substrate.
- 900SP: This is an 900 nm OD4 short-pass filter. It is Edmund Optics part #64-335. It is 25 mm in diameter and 3 mm thick. It has dielectric coatings on a fused silica substrate.
- 550LP: This is an 550 nm OD4 long-pass filter. It is Edmund Optics part #62-984. It is 25 mm in diameter and 3 mm thick. It has dielectric coatings on a fused silica substrate.
- P0: This is a window. It is Edmund Optics part #48-066. It is 25 mm in diameter and 3 mm thick. It has Edmund UV-VIS coatings on a fused silica substrate.
- 470/10, 501/8, 515/10, 640/10, 656/3, and 656/8: These are narrow-band filters, named for their approximate central wavelength and width in nm. They are off-the-shelf filters acquired from Custom Scientific. They are 25 mm in diameter and 3 mm thick. They have dielectric coatings on a fused silica substrate.

The 470/10 filter was damaged in April 2023. The central screw in wheel A came loose, jammed in filter wheel B, and scratched the 470/10 filter. Figure 15.4. We are seeking to buy a replacement.

In addition to these, we have 486/8 and 501/3 filters that could be installed by special request. Furthermore, Custom Scientific have 672/3, 672/8, and 889/18 filters that could be purchased for about US\$500 each.

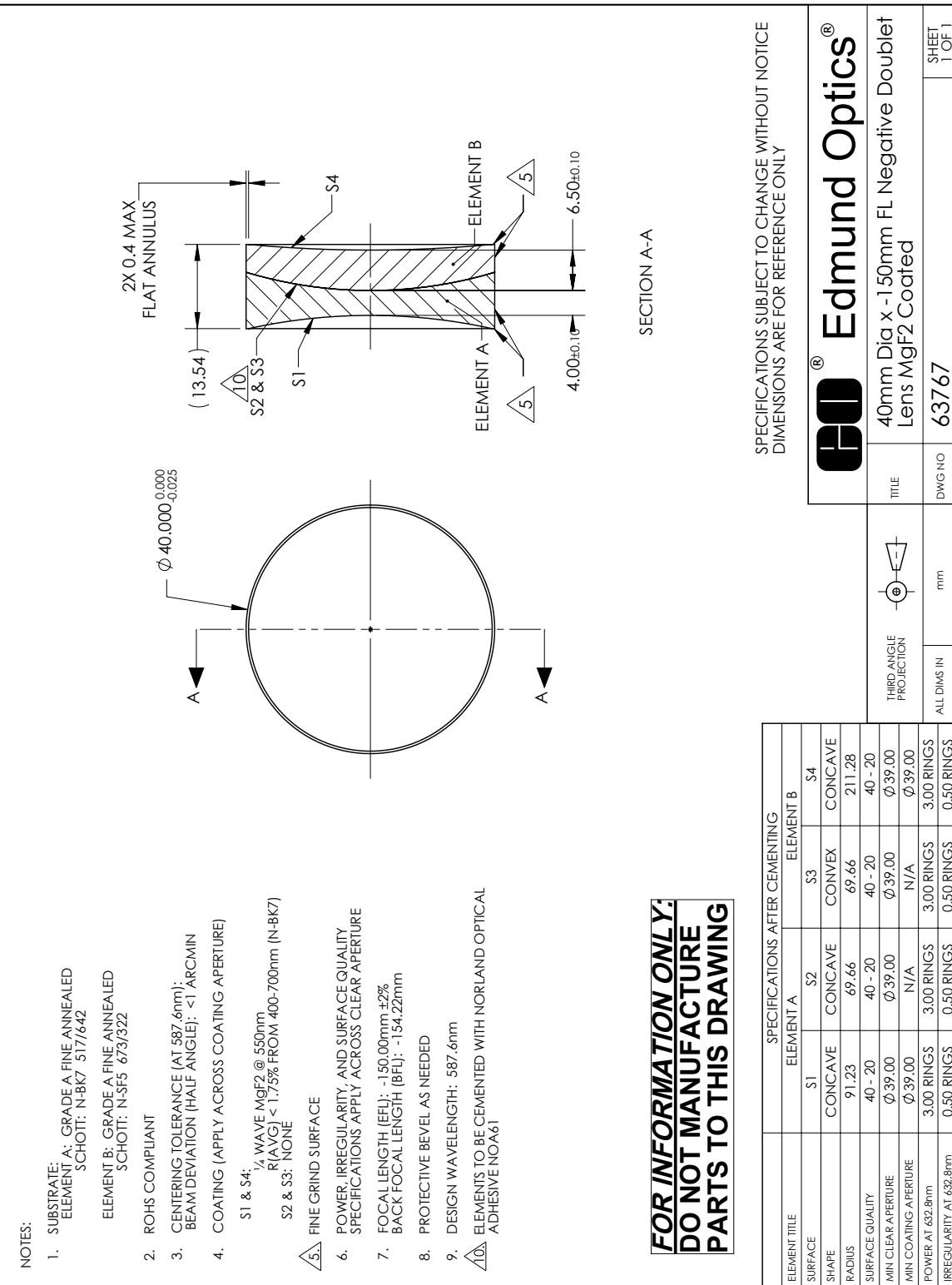


Figure 15.3: The lens design.

Table 15.1: Filter Wheel Loading

Slot	A	B	C
0	open	P0	open
1	<i>B</i>	656/3	<i>g</i>
2	<i>V</i>	470/10	<i>r</i>
3	<i>R</i>	<i>z</i>	<i>i</i>
4	825SP	<i>I</i>	550LP
5		925LP	900SP
6		515/10	656/8
7		640/10	501/8

Table 15.2: Filter Combinations

Filter	A	B	C	Thickness (mm)
dark	<i>B</i>	<i>z</i>	656/8	13
open	open	P0	open	3
<i>g</i>	open	P0	<i>g</i>	8
<i>r</i>	open	P0	<i>r</i>	8
<i>i</i>	open	P0	<i>i</i>	8
<i>z</i>	open	<i>z</i>	open	5
<i>y</i>	open	925LP	550LP	6
<i>w</i>	825SP	P0	550LP	11
<i>B</i>	<i>B</i>	P0	open	8
<i>V</i>	<i>V</i>	P0	open	8
<i>R</i>	<i>R</i>	P0	open	8
<i>I</i>	open	<i>I</i>	open	5
<i>I<sub>s</sub></i>	open	<i>I</i>	900SP	8
470/10	open	470/10	open	3
501/8	open	P0	501/8	6
515/10	open	515/10	open	3
640/10	open	640/10	open	3
656/3	open	656/3	open	3
656/8	open	P0	656/8	6



Figure 15.4: The damaged 470/10 filter.

The filter bandpasses are created by combinations of conventional bandpass filters, long-pass, and short-pass filters. The combinations used are given in Table 15.2. Most of the combinations are straightforward, but we comment on three aspects in particular:

- $I_s$ : The system responses in both  $I$  and  $I_s$  have their blue edge defined by RG9 glass. However, in  $I$  the red edge is defined by the CCD but in  $I_s$  (“ $I$  short”) it is defined by the 900SP filter. This gives  $I_s$  a system response that is a better match that of Cousins (1978), whose  $I$  has its the red edge defined by the cutoff of a GaAs photocathode around 900 nm. Compare Figure 15.8 here with Figure 9 of Bessell & Murphy (2012).
- $w$ : The  $w$  filter essentially encompasses the bandpasses of  $r$  and  $i$  (although the exact edges are slightly different). Note that this is different to Pan-STARRS  $w$  which includes the  $g$  band too. It is mainly intended for sensitive imaging of GRBs.
- P0: The role of the P0 (“prism 0”) element might seem to be a puzzle. However, we are considering converting the telescope to an altitude-azimuth configuration at some point in the future and installing wedged windows P1 and P2, similar to P0, in wheel B in place of two of the narrow-band filters. This will allow us to implement an atmospheric dispersion corrector for the  $BVR$  and  $griw$  filters using P0, P1, and P2. However, while the telescope is in an equatorial configuration, there is no point in installing P1 and P2. We could have left the position occupied by P0 as open, but we decided to install

it to give consistent bandpasses in these filters in both the equatorial and altitude-azimuth configurations.

Model system efficiency curves at the zenith (including the atmosphere, telescope mirrors, lens, filters, detector window, and detector, but excluding the obscuration of the secondary) are shown in Figures 15.5 to 15.24.

Table 15.3 gives the model properties of the filter. The filter pivot wavelength  $\lambda_{\text{pivot}}$  is defined by

$$\lambda_{\text{pivot}} \equiv \sqrt{\frac{\int \lambda S d\lambda}{\int S/\lambda d\lambda}}.$$

For a discussion of the interpretation of the pivot wavelength, see §A2.1 of Bessell & Murphy (2012). The filter FWHM is defines as the width over which  $S$  is at least half its maximum. The filter ZP is the expected electron count rate for a star with AB = 0,

$$ZP \equiv A \int SF_\lambda/(hc/\lambda) d\lambda,$$

in which  $A$  is the geometric area of the telescope (the area of the primary mirror not occulted by the secondary obscuration) and  $F_\lambda$  is the flux density of a source with  $F_\nu = 3631$  Jy.

We are monitoring photometric standards from Oke & Gunn (1983) to verify the theoretical zero-points and sensitivity curves presented above. Initial results suggest that the zero points in the blue are approximately correct, but beyond about 600 nm the observed sensitivity is only about 75% of the theoretical sensitivity.

## 15.4 Focuser and Rotator

The instrument incorporates an Optec Gemini focuser and rotator between the last filter wheel and the detector.

The focuser moves from 0 to 115200 steps over 12.7 mm which corresponds to 9.07 steps per micron. The 0 position is above and the 115200 position is below. The focuser moves at about 900 steps or 0.1 mm per second.

## 15.5 Focus Compensation

The lens has chromatic aberration and the filters have different thicknesses. Both of these require us to use a compensator to maintain focus. Our options are the focuser, the secondary, or both. If we use only one compensator, then the magnification necessarily changes slightly was we adjust for focus. If we use both, we can maintain the magnification.

However, it is fairly easy to show that if we use the focuser, either on its own or in combination with the secondary to maintain the magnification, in the worst case we need to move it about 3 mm. Since the focuser moves at about 0.1 mm per second, this means the worse case time is about 30 seconds. This is long compared to slew speed (without a meridian flip) and cannot

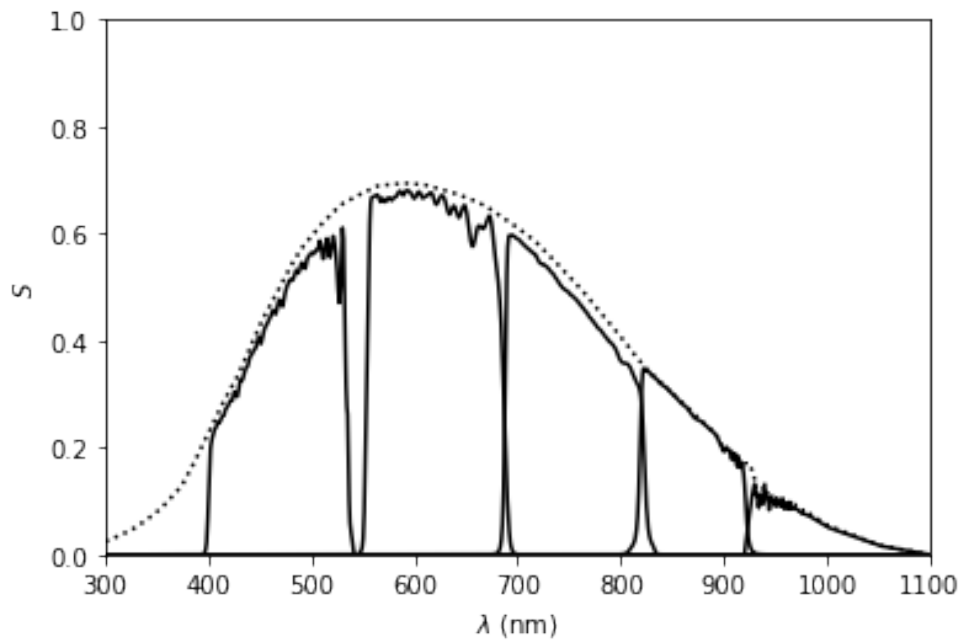


Figure 15.5: The model system efficiency  $S$  at the zenith in the *grizy* filters. The dotted line is the model unfiltered efficiency.

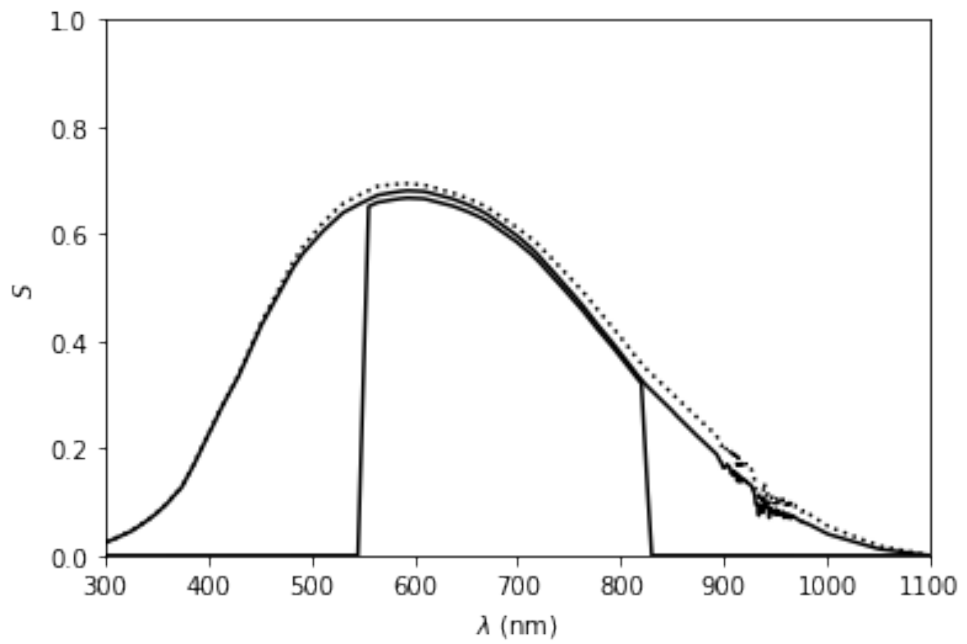


Figure 15.6: The model system efficiency  $S$  at the zenith in the *w* and open filters. The dotted line is the model unfiltered efficiency.

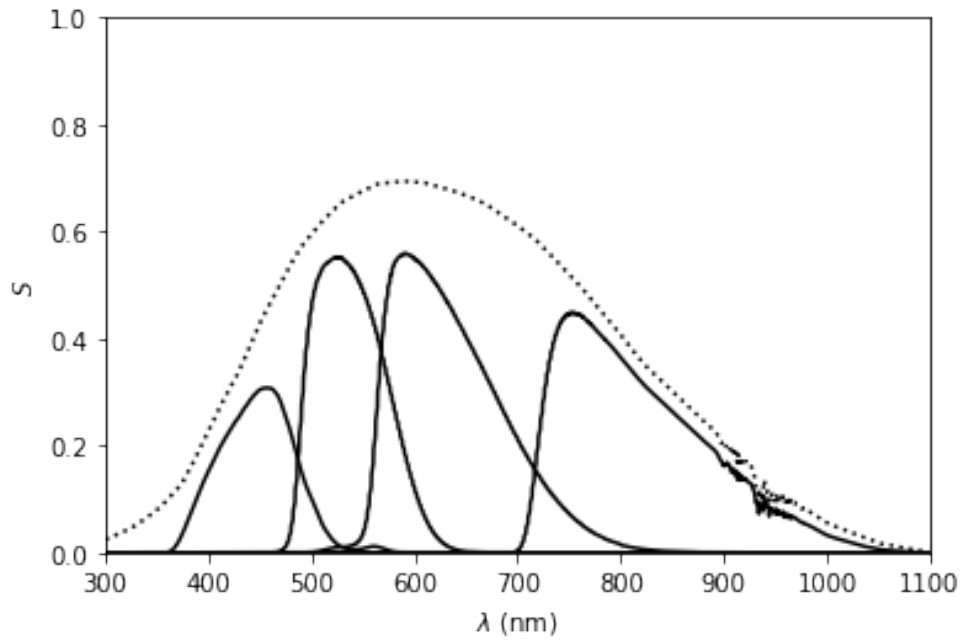


Figure 15.7: The model system efficiency  $S$  at the zenith in the  $BVRI$  filters. The dotted line is the model unfiltered efficiency.

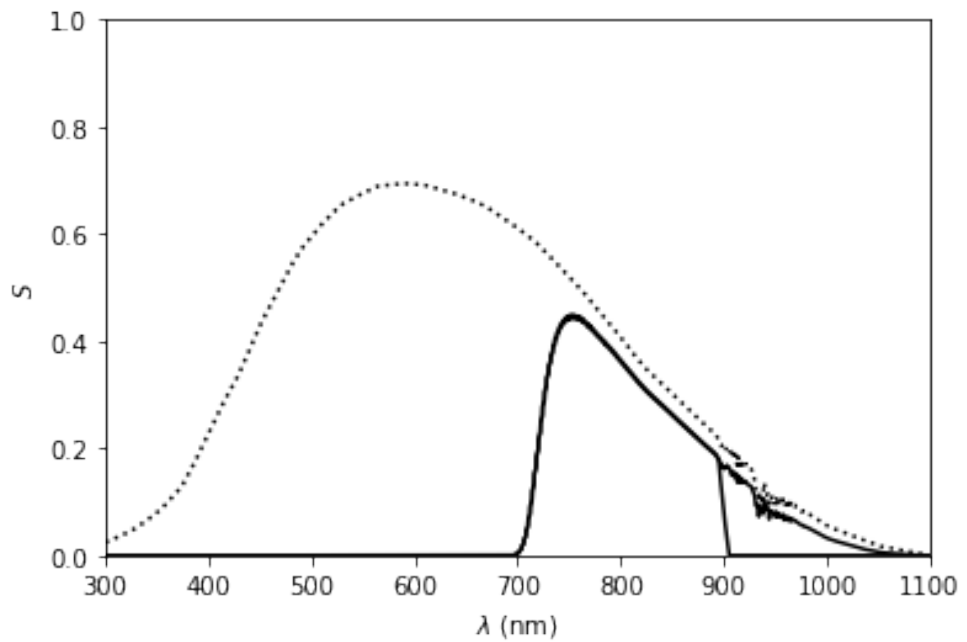


Figure 15.8: The model system efficiency  $S$  at the zenith in the  $I$  and  $I_s$  filters. The  $I_s$  filter has a red cutoff defined by the 900SP filter whereas the  $I$  filter has the red cutoff defined by the CCD. The dotted line is the model unfiltered efficiency.

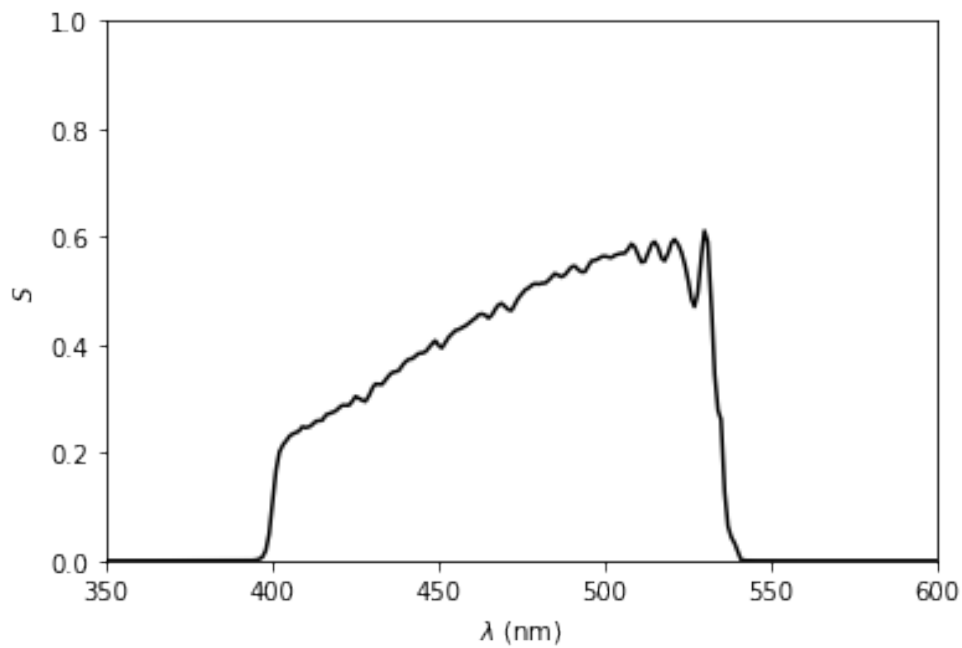


Figure 15.9: The model system efficiency  $S$  at the zenith in the  $g$  filter.

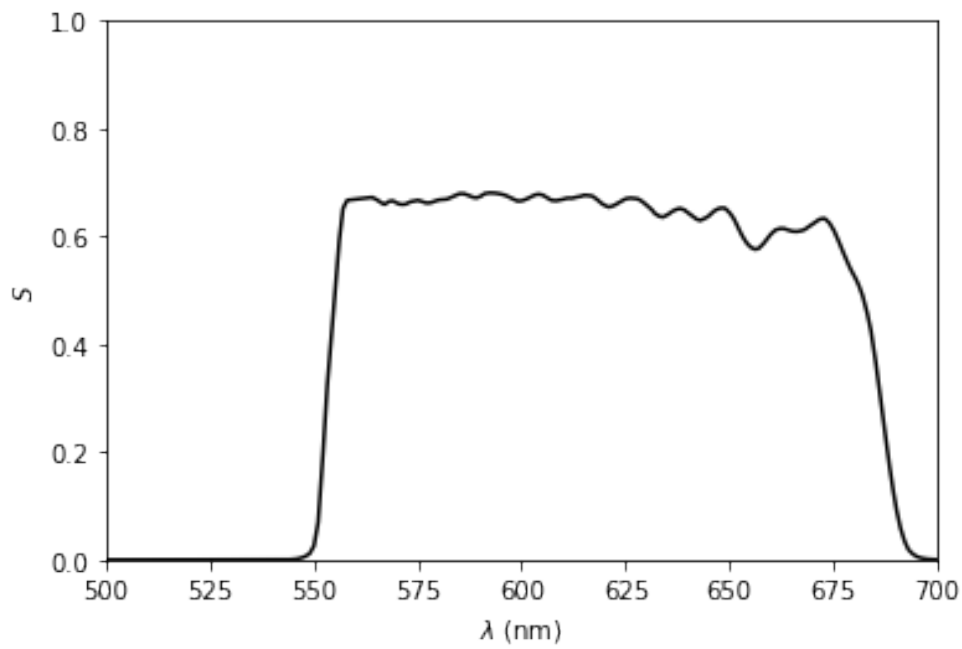


Figure 15.10: The model system efficiency  $S$  at the zenith in the  $r$  filter.

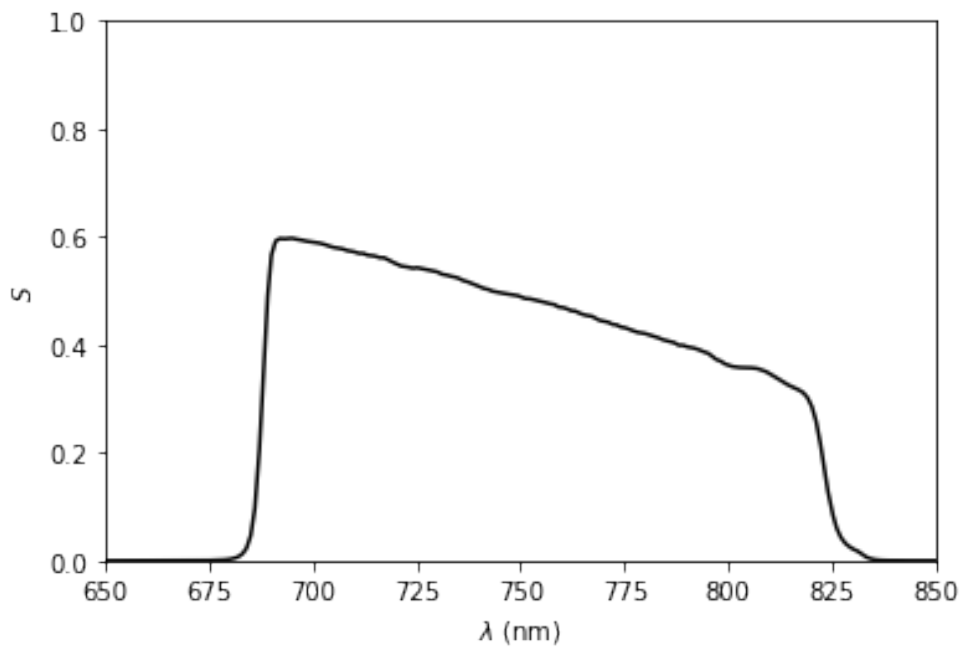


Figure 15.11: The model system efficiency  $S$  at the zenith in the  $i$  filter.

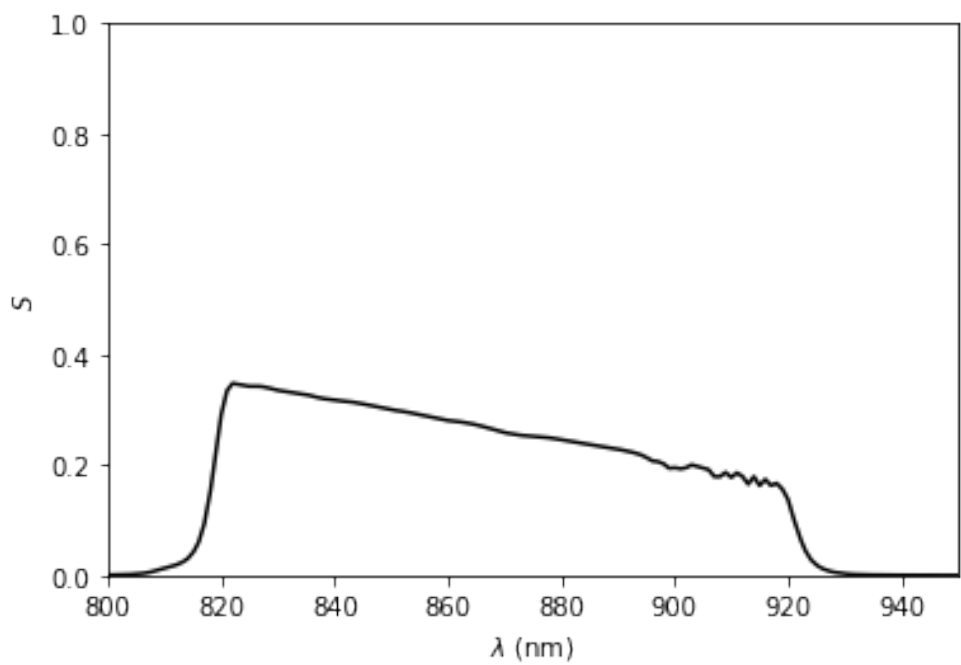


Figure 15.12: The model system efficiency  $S$  at the zenith in the  $z$  filter.

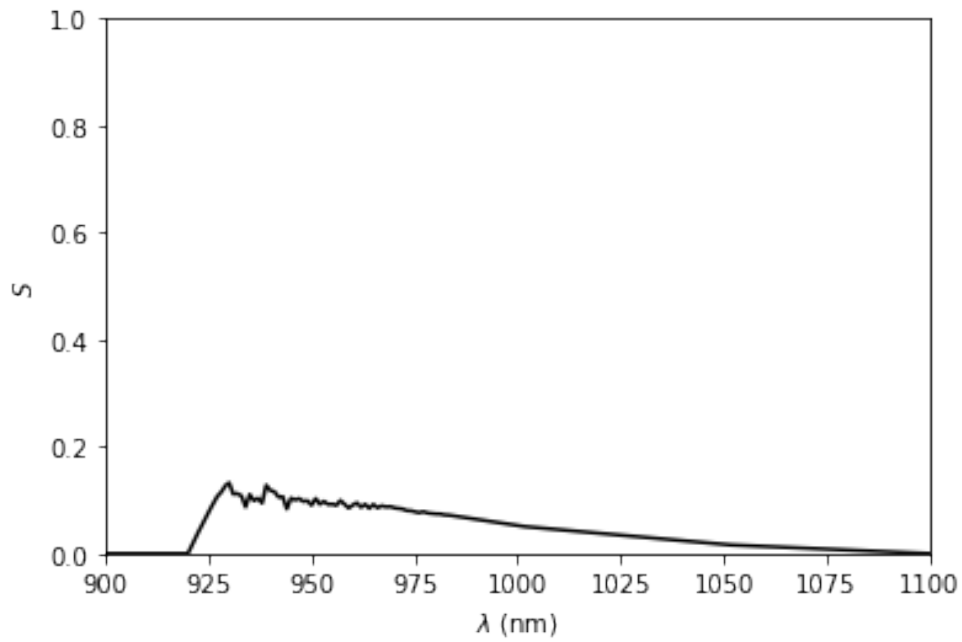


Figure 15.13: The model system efficiency  $S$  at the zenith in the  $y$  filter.

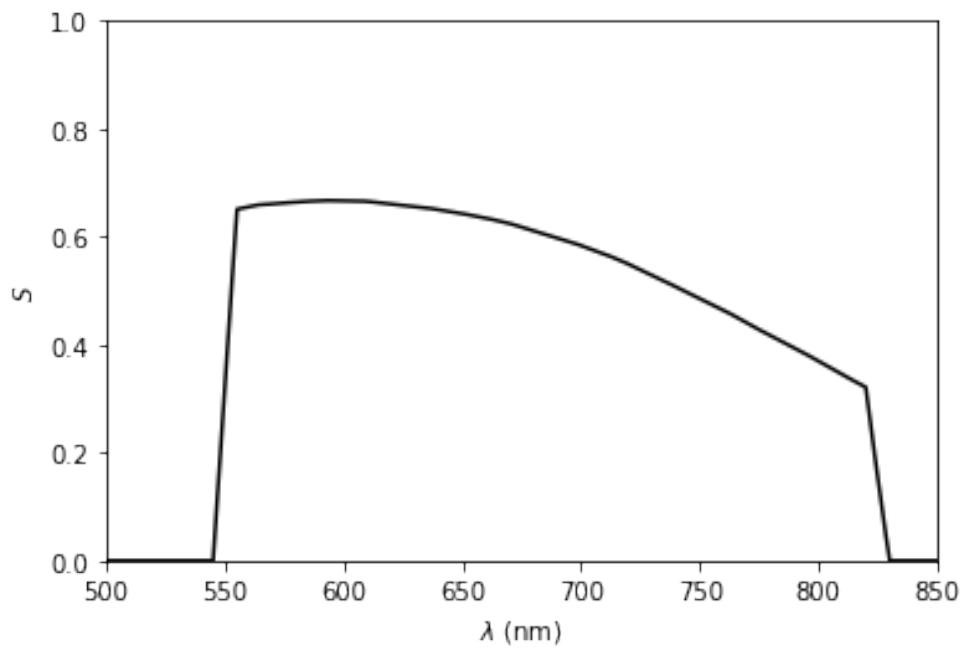


Figure 15.14: The model system efficiency  $S$  at the zenith in the  $w$  filter.

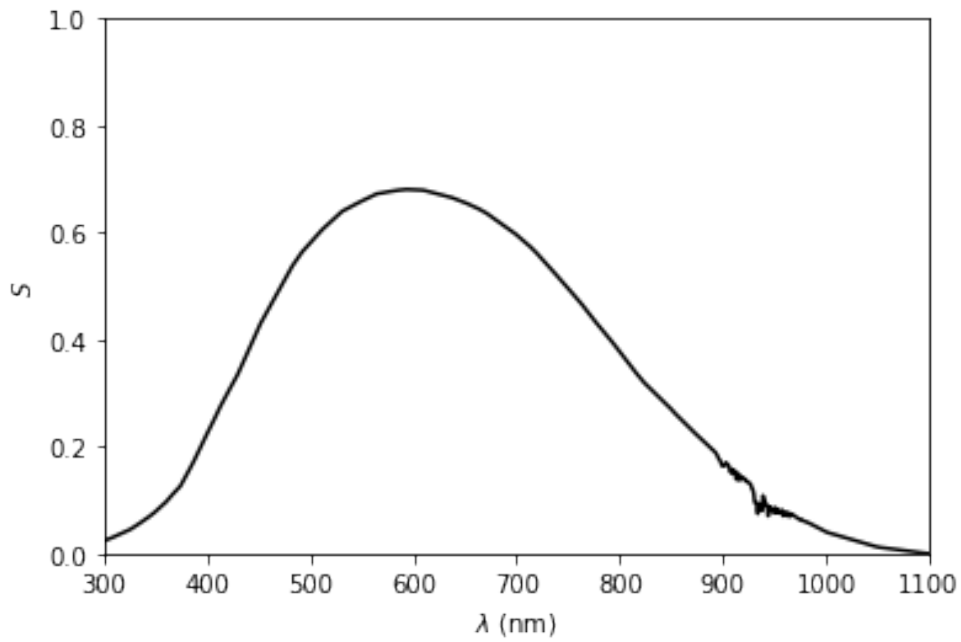


Figure 15.15: The model system efficiency  $S$  at the zenith in the open filter.

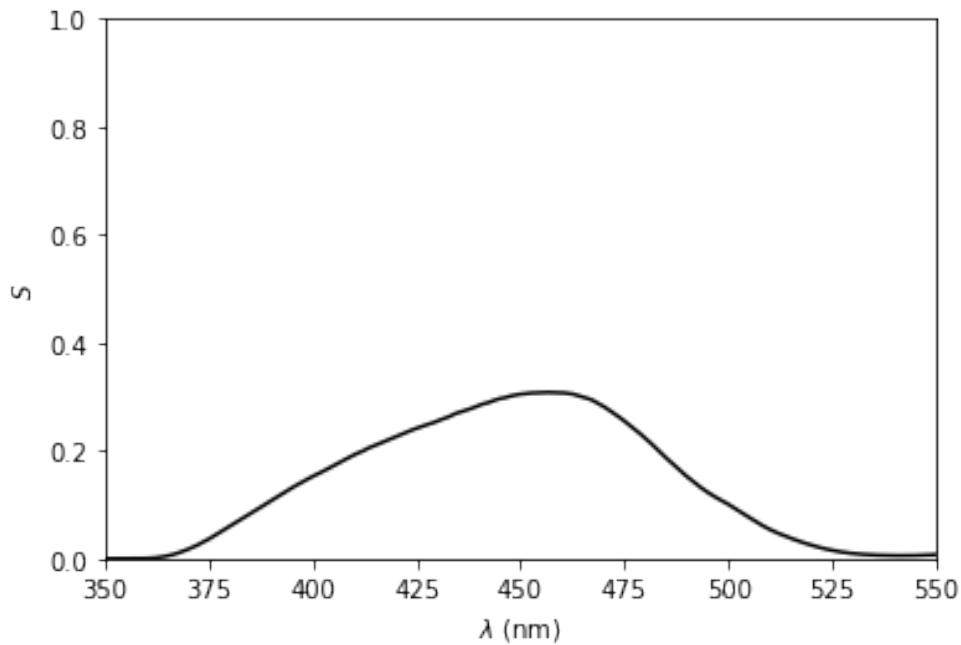


Figure 15.16: The model system efficiency  $S$  at the zenith in the  $B$  filter.

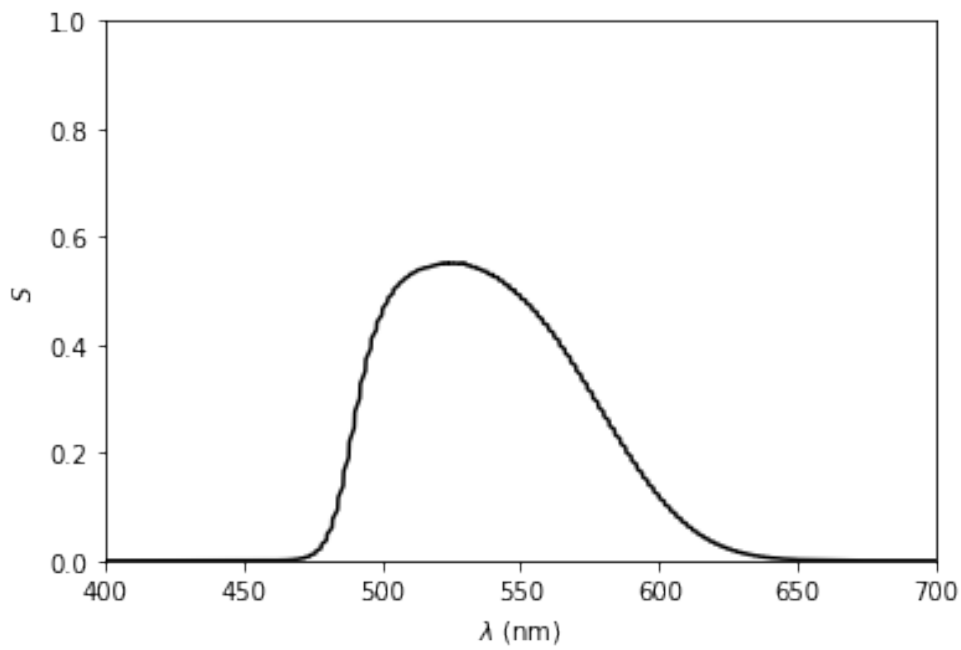


Figure 15.17: The model system efficiency  $S$  at the zenith in the  $V$  filter.

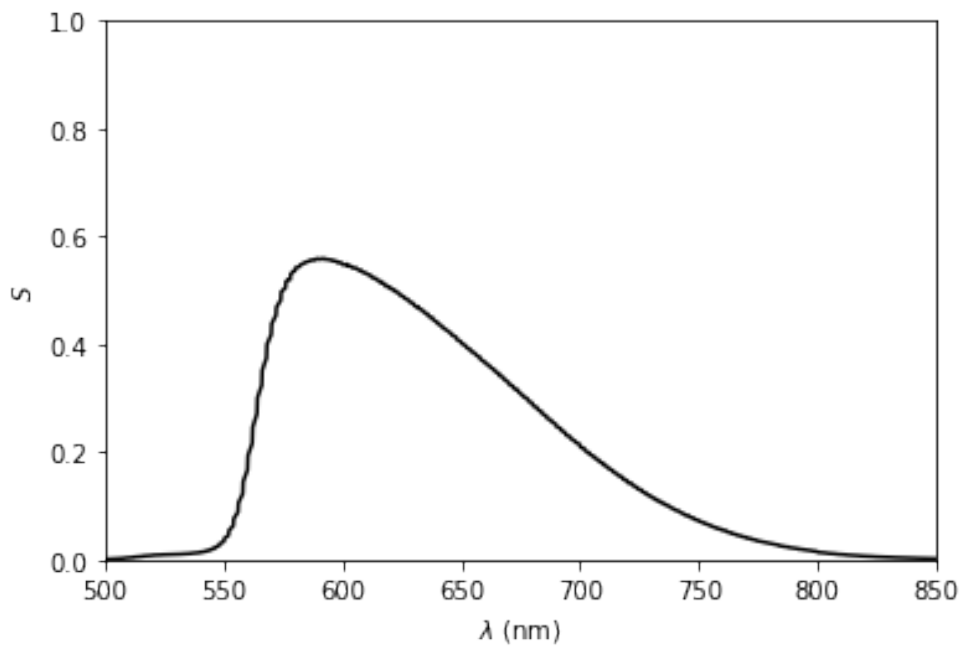


Figure 15.18: The model system efficiency  $S$  at the zenith in the  $R$  filter.

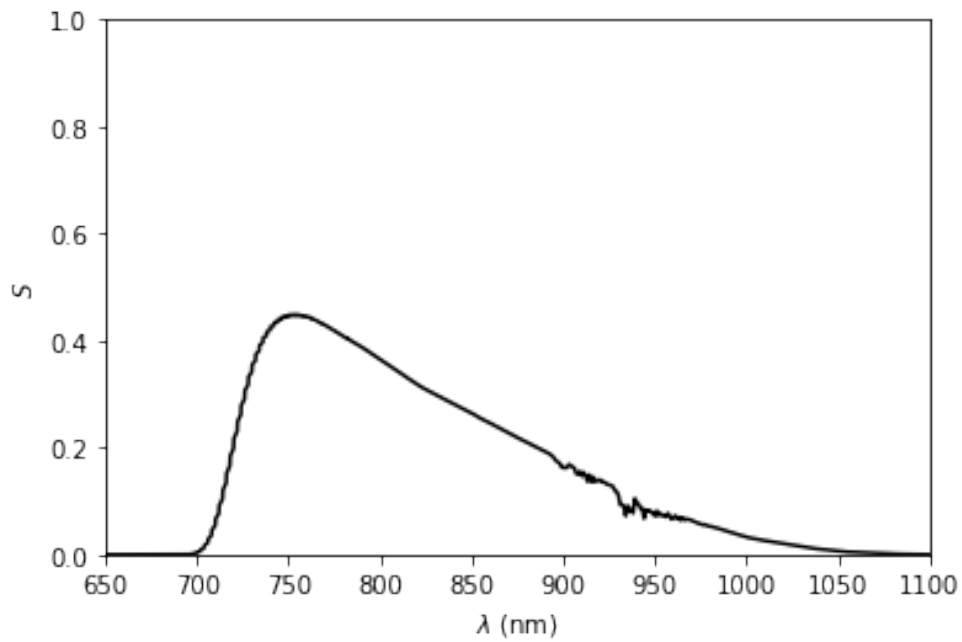


Figure 15.19: The model system efficiency  $S$  at the zenith in the  $I$  filter.

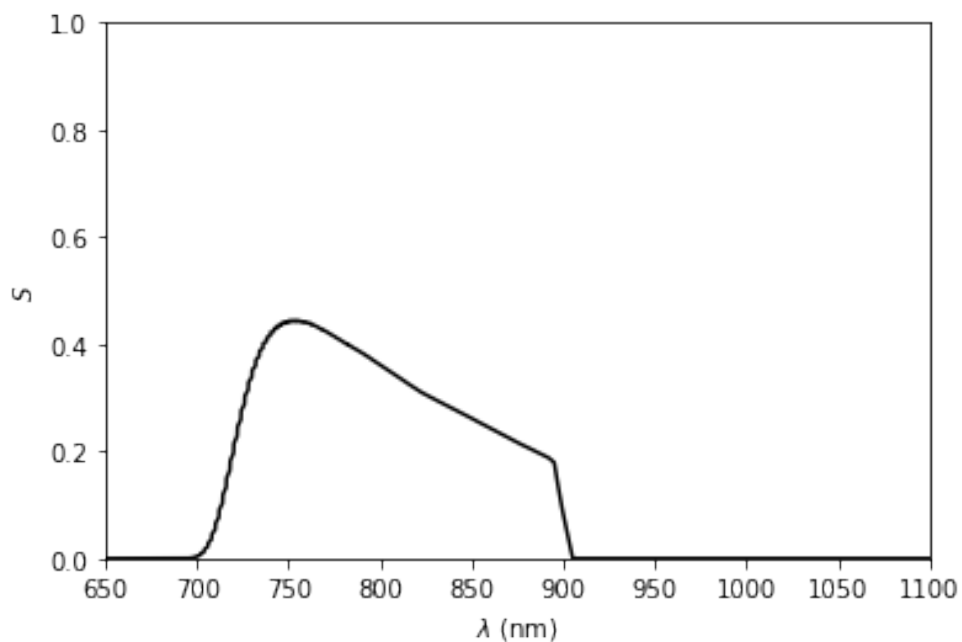


Figure 15.20: The model system efficiency  $S$  at the zenith in the  $I_s$  filter.

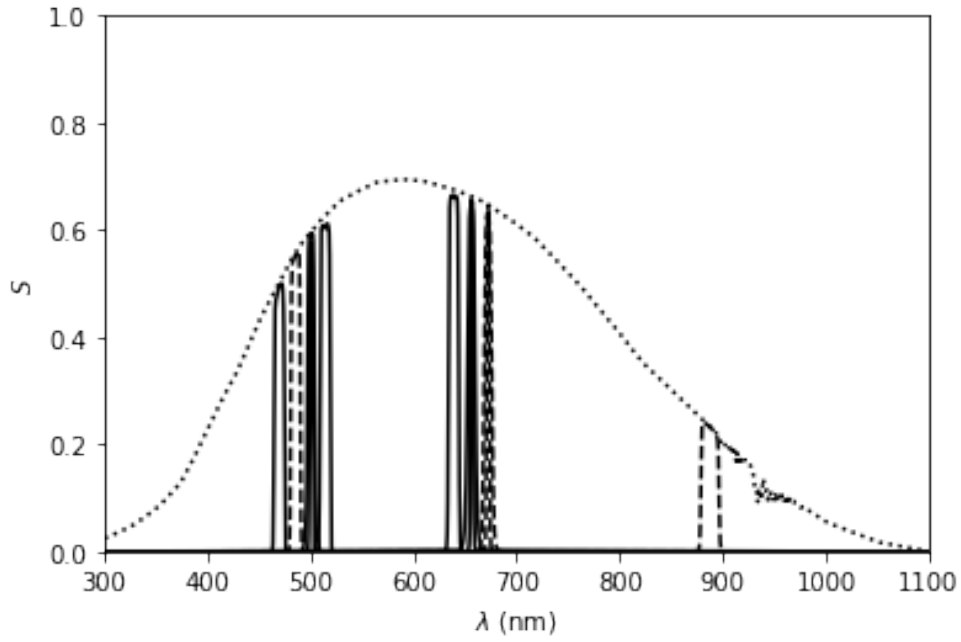


Figure 15.21: The model system efficiency  $S$  at the zenith in the narrow-band and medium-band filters. The dotted line is the model unfiltered efficiency.

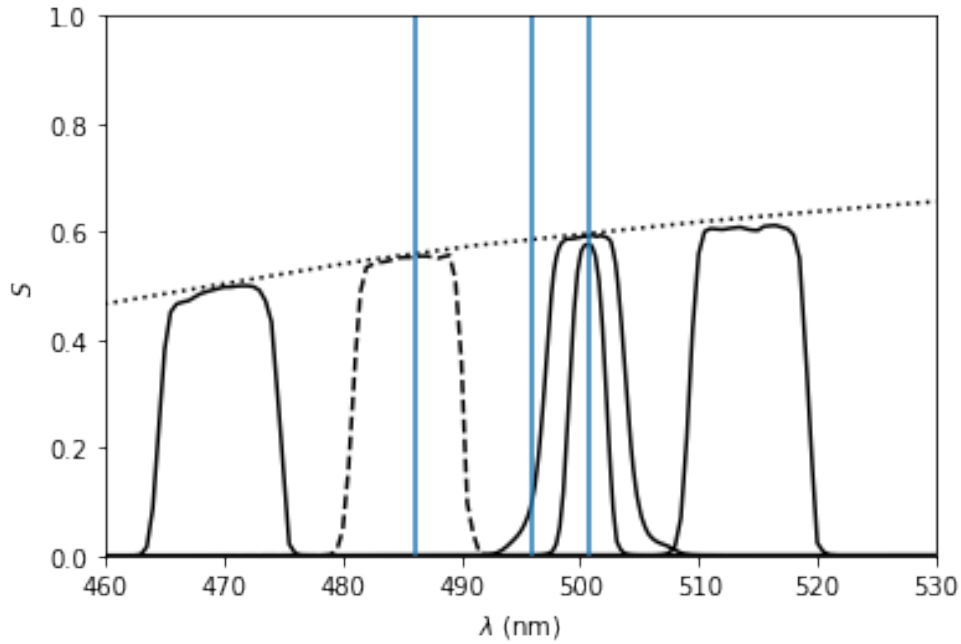


Figure 15.22: The model system efficiency  $S$  at the zenith in the narrow-band and medium-band filters in  $g$ : 470/10, 486/8, 501/3, 501/8, and 515/10. The filters shown with dashed lines have not yet been acquired. The dotted line is the model unfiltered efficiency. The blue vertical lines are at 486.1, 495.9, and 500.7 nm.

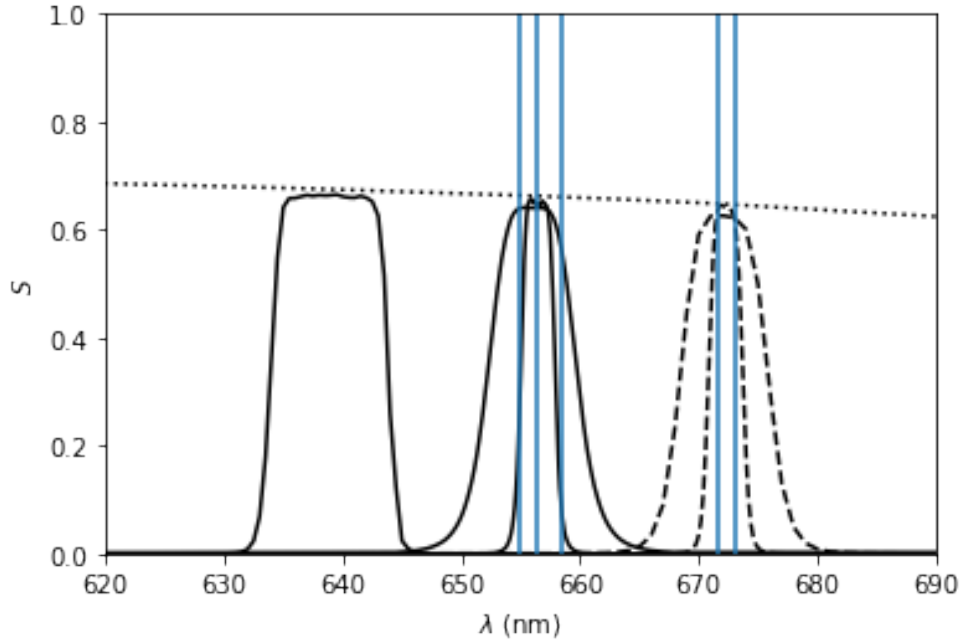


Figure 15.23: The model system efficiency  $S$  at the zenith in the narrow-band and medium-band filters in  $r$ : 640/10, 656/3, 656/8, 672/3, and 672/8, 501/8, and 515/10. The filters shown with dashed lines have not yet been acquired. The dotted line is the model unfiltered efficiency. The blue vertical lines are at 656.3, 654.8, 658.4, 671.6, and 673.1 nm.

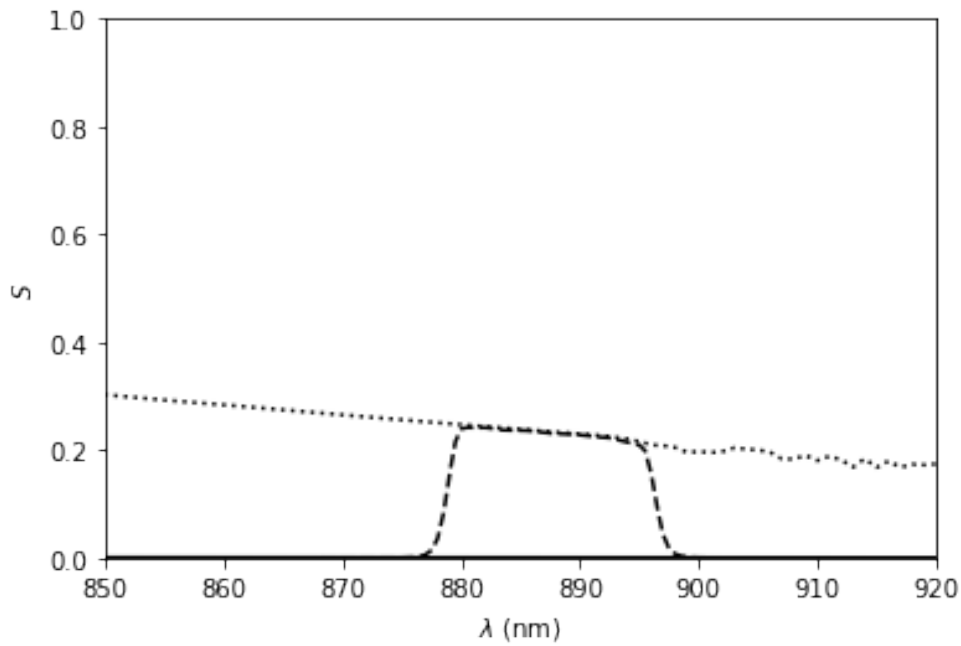


Figure 15.24: The model system efficiency  $S$  at the zenith in the medium-band filter in  $z$ : 889/18. The filters shown with dashed lines have not yet been acquired. The dotted line is the model unfiltered efficiency.

Table 15.3: Model Filter Properties

Filter	$\lambda_{\text{pivot}}$ (nm)	$\Delta\lambda$ (nm)	ZP ( $\text{s}^{-1}$ )
open	618.7	384.1	$4.2 \times 10^9$
<i>g</i>	475.9	104.6	$1.2 \times 10^9$
<i>r</i>	617.2	132.4	$1.3 \times 10^9$
<i>i</i>	747.4	131.5	$8.0 \times 10^8$
<i>z</i>	862.8	94.8	$3.0 \times 10^8$
<i>y</i>	973.3	64.2	$8.6 \times 10^7$
<i>w</i>	668.4	264.6	$2.2 \times 10^9$
<i>B</i>	446.5	89.4	$5.9 \times 10^8$
<i>V</i>	537.9	89.8	$8.5 \times 10^8$
<i>R</i>	633.9	118.0	$1.0 \times 10^9$
<i>I</i>	814.8	150.7	$8.0 \times 10^8$
<i>I<sub>s</sub></i>	795.0	150.7	$7.0 \times 10^8$
470/10	469.7	10.1	$9.9 \times 10^7$
486/8	485.5	9.3	$1.0 \times 10^8$
501/3	500.7	3.2	$3.5 \times 10^7$
501/8	500.5	7.0	$8.2 \times 10^7$
515/10	514.2	10.0	$1.1 \times 10^8$
640/10	638.9	9.9	$9.8 \times 10^7$
656/3	656.5	2.9	$2.8 \times 10^7$
656/8	655.9	7.7	$8.4 \times 10^7$
672/3	672.3	2.9	$2.7 \times 10^7$
672/8	672.2	7.6	$6.8 \times 10^7$
889/18	887.3	17.5	$4.3 \times 10^7$

be overlapped with changing the filter. On the other hand, if we use only the secondary, in the worst case we need to move about 60 steps. Even with backlash compensation, this takes about 5.5 seconds. Furthermore, this can be overlapped with changing the filter. Therefore, in the interests of preserving the rapid response of COATLI, we have chosen to compensate the focus using only the secondary. This compensation is handled automatically by the control system.

Our model is as follows. We define  $L$  to be the (fixed) physical distance from the lens to the detector and  $T$  to be the total physical thickness of filter glass between the lens and the detector. We then have

$$SA' = L - [(n - 1)/n]T \approx L - 0.32T,$$

where we have assumed  $n = 1.48$  for fused silica. We then solve for SA using

$$1/F = 1/SA' - 1/SA,$$

taking into account the dependence of  $F$  on wavelength. We determine  $\Delta SA$  relative to the *i* filter. We then determine the corresponding change in the secondary taking into account the amplification of 10.64 between the movement of the secondary and the movement of the telescope focal plane.

Table 15.4 shows the results. Note that for the medium band filters, there are two values depending on whether the filter is in wheel B ( $T = 3$  mm) or wheel C ( $T = 6$  mm). The offsets

of the narrowband filters are the same as for the corresponding medium band filters.

## 15.6 Detector

The detector unit is an Andor iXon Ultra 888 with an e2v CCD201-20 electron-multiplying CCD detector. The detector was acquired in 2014 and originally intended to be the tilt sensor for the planned two-channel imager.

### 15.6.1 Format, Scale, and Field

The detector has  $1024 \times 1024$  pixels each  $13 \times 13 \mu\text{m}$  square. The detector gives a pixel scale of 0.269 arcsec and a field of 4.59 arcmin.

The orientation of the field on the sky depends on the mount rotation (given by the values of the SMTMRO and EMTMRO keywords in the header), and is shown in Figure C.2. However, the pipeline reduction rotates all images to the conventional orientation with north up and east left.

### 15.6.2 Quantum Efficiency

The detector has standard silicon and the e2v midband coating (which in Andor's terminology makes it a "BV" device).

Table 15.4: Filter Secondary Offsets

Filter	<i>F</i> (mm)	Thickness (mm)	Offset (steps)
open	-150.22	3	-24
<i>g</i>	-150.20	8	+7
<i>r</i>	-150.07	8	+13
<i>i</i>	-150.37	8	0
<i>z</i>	-150.66	5	-30
<i>y</i>	-150.96	6	-37
<i>w</i>	-150.25	11	+24
<i>B</i>	-150.43	8	-2
<i>V</i>	-150.97	8	+17
<i>R</i>	-150.14	8	+10
<i>I</i>	-150.27	5	-30
<i>I<sub>s</sub></i>	-150.50	8	-5
470/10	-149.99	3/6	-14/+4
515/10	-149.93	3/6	-12/+6
640/10	-150.07	3/6	-16/+1

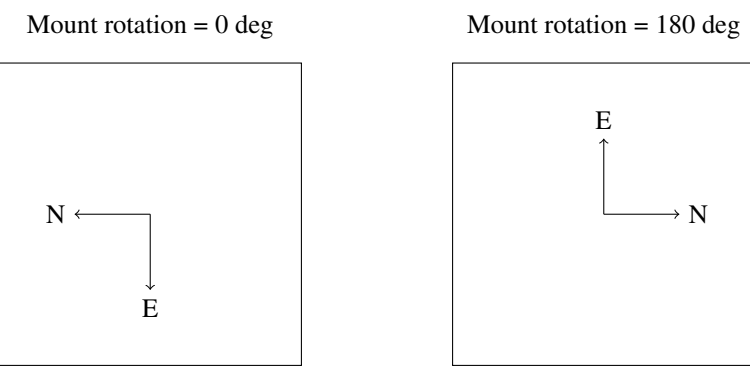


Figure 15.25: The orientation of the detector on the sky according to the mount rotation. The pixel origin is in the lower left.

The nominal quantum efficiency is shown in Figure C.3. The detector has excellent efficiency from 500 to 800 nm.

### 15.6.3 Readout Architecture

The detector can be read using either a conventional signal chain (at 100 kHz or 1 MHz) or an EM signal chain (at 1, 10, 20, or 30 MHz). Both chains have two gains and the EM gain can be set to up to 1000.

Although the conventional and EM amplifiers clock the serial register in different directions, the control software flips each row in conventional data so that physical pixels have the same logical position in the FITS files.

The detector is used in frame-transfer mode without a mechanical shutter (see §C.2.4). At the end of an exposure, the charge is rapidly clocked into from the light-sensitive image section to the shielded store section. The charge can then be read. In EM mode, the next exposure can then start immediately.

With the normal vertical-shift frequency of 4.33 MHz, the frame transfer takes about 4.5 ms. This leads to some trailing above and below bright stars.

The read-out architecture has several parameters, which are encoded in the value of the READMODE header keyword. The value is a string of the form *A-B-C-D-E-F-G* in which *A* to *G* are non-negative integers with the following meanings:

- A* The ADC channel index. This is always 0 since the detector only has one ADC channel.
- B* The amplifier index. This is 0 for the EM amplifier and 1 for the conventional amplifier.
- C* The vertical shift speed index. For both amplifiers, 0 is 0.60 MHz, 1 is 1.13 MHz, 2 is 2.20 MHz, and 3 is 4.33 MHz.
- D* The horizontal shift speed index. For the EM amplifier, 0 is 30 MHz, 1 is 20 MHz, 2 is 10 MHz, and 3 is 1 MHz. For the conventional amplifier, 0 is 1 MHz and 1 is 100 kHz.
- E* The gain index. For both amplifiers, 0 is low gain (more electrons per ADU) and 1 is high gain (fewer electrons per ADU).
- F* The nominal EM gain. This is ignored when the conventional amplifier is used. For the EM amplifier, it can be between 1 and 1000.
- G* The software gain. After the data are read, each ADU signal is divided by the software gain to reduce white noise in the low-order bits (see Watson 2002, RMAA, 38, 233).

Fortunately, there is little need to use these values directly, since aliases are defined for common modes. They are shown in Table C.1.

### 15.6.4 Shutter and Dark Filter

We originally attempted to use the mechanical shutter for conventional CCD modes and the frame-transfer capability for EM modes. However, we found that the shutter sometimes failed to open or failed to open completely. We suspect that at the colder temperatures of winter nights night, the power supply does not provide sufficient voltage to open the shutter.

Therefore, we now leave the shutter open between exposures and use the frame-transfer capability in both conventional and EM modes. As noted above, with the normal vertical-shift frequency, the frame transfer takes about 4.5 ms.

Note that the shutter closes when the detector head is powered down. This sometimes occurs at night, as the detector head sometimes becomes uncommunicative and is automatically powered down and up again by the control system. There is a risk that after such a cycle the shutter will not open or not open completely.

To take bias and dark images, we have use a “dark” filter that consists of the *B*, *z*, and 656/8 filters in series. Despite this, light leaks in the filter wheel mean that we need to take biases and darks at night.

## 15.7 Mechanics

Figures 15.27 and 15.29 show an overall view of the instrument mechanics. Figures 15.30 to 15.44 show drawings of the individual parts.

One detail that is not shown in the drawings are the internal baffles. On the lower sides of filter wheels A and B we have installed FLI-supplied adapters as shown in Figure 15.46. Within these we have placed two black nylon baffles, shown in Figure 15.44, to reduce scattered light.

TODO: Cable clamps. M5×0.8 thread. Use 4 mm hex key.

## 15.8 Procedures

### 15.8.1 Dismounting the Instrument

#### Requirements

You will need:

- Two persons.
- The key to the shed.
- 4 mm and 5/64-inch hex keys.
- 2 mm flat-bladed screwdriver.
- Cutting pliers.
- 8 mm wrench

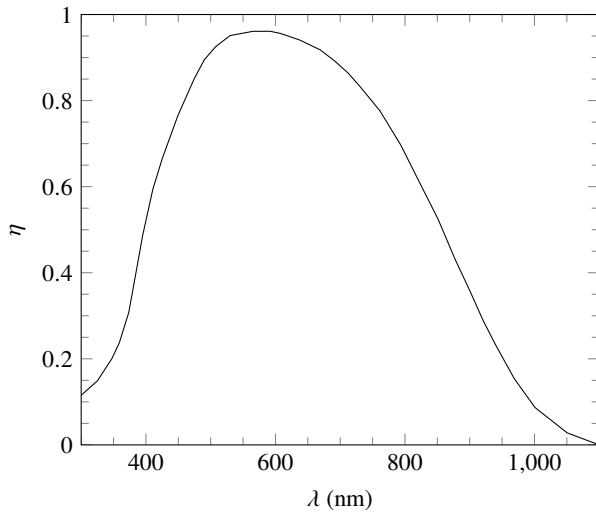


Figure 15.26: The nominal quantum efficiency  $\eta$  of the Huitzi detector.

Table 15.5: Read-Mode Aliases

Alias	Mode
initial	default
default	em-30MHz
conventionaldefault	1MHz
fastguidingdefault	em-30MHz
1MHz	1MHz-low
em-10MHz	em-10MHz-low
em-20MHz	em-20MHz-low
em-30MHz	em-30MHz-low
1MHz-low	0-1-3-0-0-1-1
1MHz-high	0-1-3-0-1-1-2
em-10MHz-low	0-0-3-2-0-250-2
em-10MHz-high	0-0-3-2-1-160-4
em-20MHz-low	0-0-3-1-0-500-4
em-20MHz-high	0-0-3-1-1-320-8
em-30MHz-low	0-0-3-0-0-1000-8
em-30MHz-high	0-0-3-0-1-640-16

Mode Name	1MHz-0	em-10MHz-0	em-20MHz-0	em-30MHz-0
Amplifier	Conventional	EM	EM	EM
Horizontal Speed	1 MHz	10 MHz	20 MHz	30 MHz
Software Gain	1	2	4	8
ADC Range (DN)	64k	32k	16k	8k
Gain ( $e^-$ /DN)	3.3	41	78	117
Read Noise (DN)	2.1	2.6	1.9	1.7
Read Noise ( $e^-$ )	7	105	145	204
Bias Level (DN)	500	242	123	62
Linear Limit ( $e^-$ )		400k	400k	400k
Saturation (DN)	58k	32k	16k	8k
Saturation ( $e^-$ )	190k	1300k	1250k	940k
Linearity ( $e^-$ )		400k	400k	400k
Linearity (DN)		9700	5100	3400
Dynamic Range (bits)		11.9	11.4	10.9

Table 15.6: Detector Characteristics with the Low Preamplifier Gain

Mode Name	1MHz-1	em-10MHz-1	em-20MHz-1	em-30MHz-1
Amplifier	Conventional	EM	EM	EM
Horizontal Speed	1 MHz	10 MHz	20 MHz	30 MHz
Software Gain	2	4	8	16
ADC Range (DN)	32k	16k	8k	4k
Gain ( $e^-$ /DN)	1.6	21	45	70
Read Noise (DN)	2.9	2.7	2.4	1.6
Read Noise ( $e^-$ )	5	56	108	115
Bias Level (DN)	250	119	62	31
Saturation (DN)	22k			
Saturation ( $e^-$ )	35k			
Linearity ( $e^-$ )		400k	400k	400k
Linearity (DN)		19000	8900	5700
Dynamic Range (bits)		12.8	11.9	11.8

Table 15.7: Detector Characteristics with the High Preamplifier Gain

Table 15.8: Mechanical Parts and Hardware

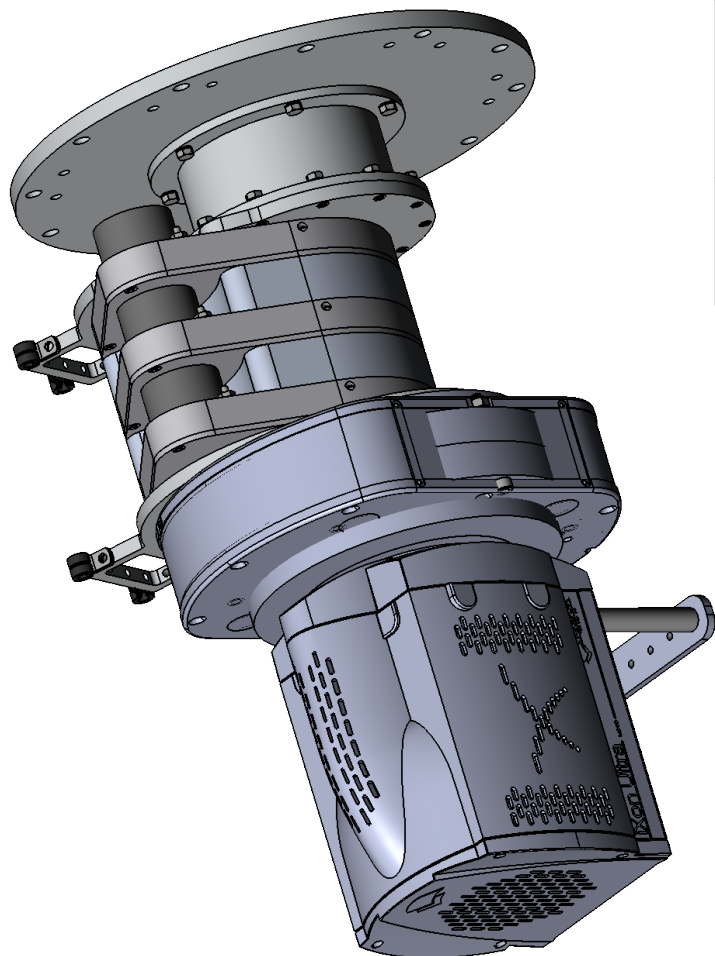
part	Name	Quantity	Notes
1	Instrument flange	1	
2	Main barrel	1	
3	Lens barrel ring	1	
4	Lens barrel	1	Edmund Optics #57-978
5	Upper filter wheel interface plate	1	
6	Filter wheel	3	FLI CFW-1-5 (A) or CFW-1-8 (B and C)
7	Filter wheel separator	2	
8	Lower filter wheel interface plate	1	
9	Upper focuser interface ring	1	
10	Focuser	1	Optec Gemini
11	Lower focuser interface ring	1	
12	Detector head	1	Andor iXon Ultra 888
13	Detector posts	2	Andor 12.7 mm diameter 80 mm long with 1/4-20 thread
14	Detector cable support plate	1	
X	Lens barrel separator	1	
?	Filter wheel adapter	2	FLI part supplied with filter wheels
Z	Internal baffle	2	Black nylon
15	SS Hex Head Screw M5×0.8×12	12	McMaster 91287A122
16	SS Belleville Spring Lock Washer M5	12	McMaster 90895A027
17	Threaded Insert M5×0.8×7.5	12	McMaster 97120A220 (= part 22)
18	Threaded rod M3×0.5	6	Modified from McMaster 90024A218
19	SS Hex Nut M3×0.5	6	McMaster 91828A211
20	SS Spring Lock Washer Conical M3	6	McMaster 91477A121
21	Thread-Lock Insert M3×0.5×6.5	6	McMaster 97120A190
22	Threaded Insert M5×0.8×7.5	4	McMaster 97120A220 (= part 17)
23	SS Socket Head Screw M5×0.8×10	8	McMaster 91292A124
24	SS Oval-Tip Set Screw 18-8 1/4-inch	6	McMaster 92778A113
25	SS Flat-Tip Set Screw 18-8 1/8-inch	6	McMaster 94355A180
26	SS Hex Socket Screw Flat Head 82 deg Countersink 1/4-20 1/2-inch	2	McMaster 92210A537
27	SS Belleville Spring Lock Washer 1/4	2	McMaster 93501A029
28	SS Hex Socket Screw Button Head M5×0.8×50	4	McMaster 92095A228
?	Hex Socket Screw M5×0.8	6	

# Huítzi

## Planos Mecánicos

(2022 - 11 - 23)

Nota: se agregó un nuevo plano  
con el separador Huítzi-ME-SS-AC-006.  
(2023 - 02 - 19)



UNLESS OTHERWISE SPECIFIED: DIMENSIONS ARE IN MILLIMETERS TOLERANCES ARE IN MILLIMETERS UNLESS OTHERWISE SPECIFIED ANGULAR: 0.05°		INCHES	DEBIR AND BREAK SHAPE EBCS	DONCH SCALE DRAWING	REVISION
NAME	SIGNATURE	DATE			12-09-2022
DRAWN	A/S	12-09-2022			
CHECKED	AW	14-09-2022			
APPROVED	NA	NA			
MEG			NA	DWG NO.	Huítzi-ME
QA			NA	SCALE	A3
			WEIGHT front SW	SCALE	1/2
					SHEET 1 OF 2

Figure 15.27: The instrument mechanics.

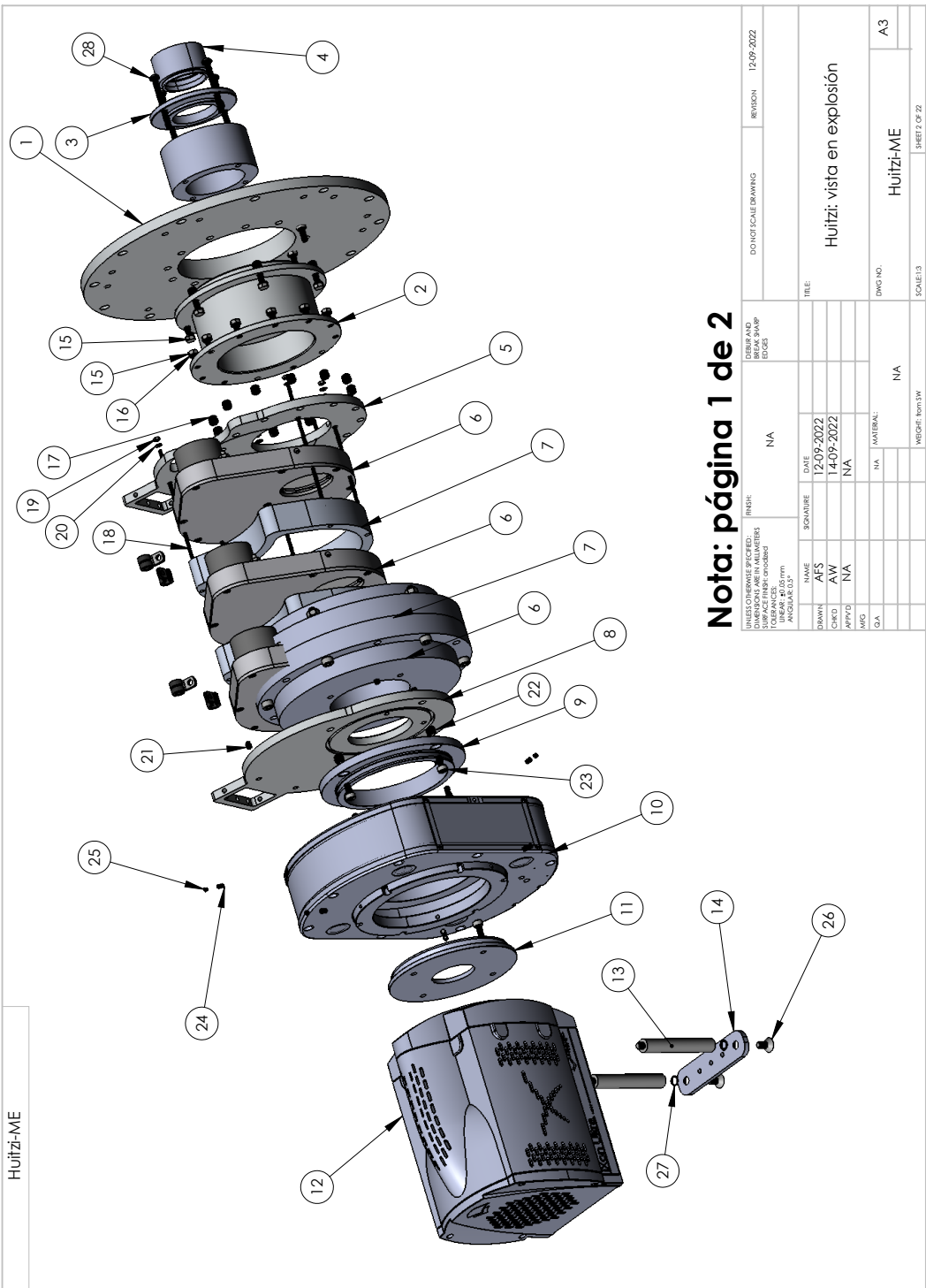


Figure 15.28: The instrument mechanics (exploded view).

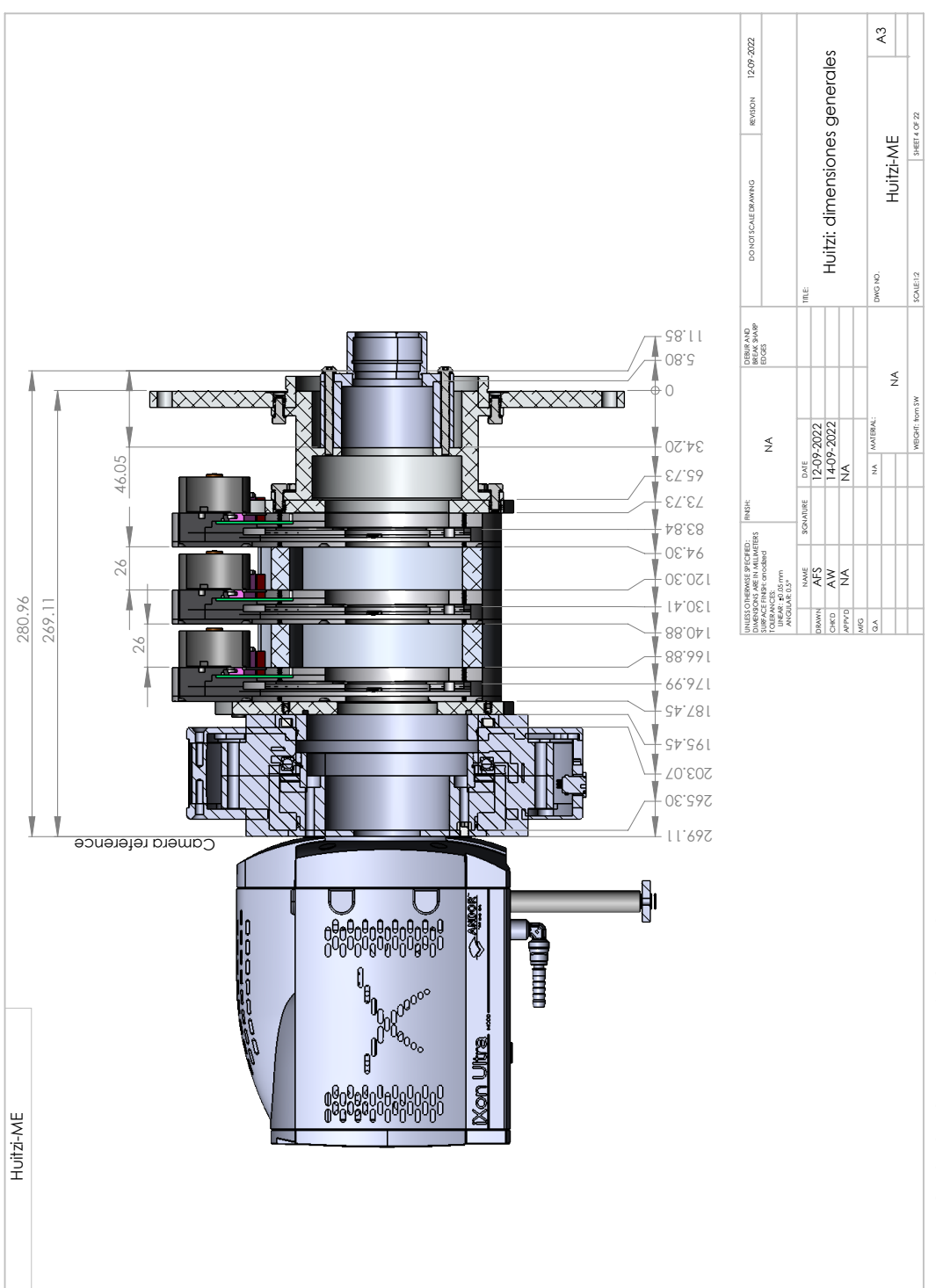


Figure 15.29: The instrument mechanics (longitudinal section).

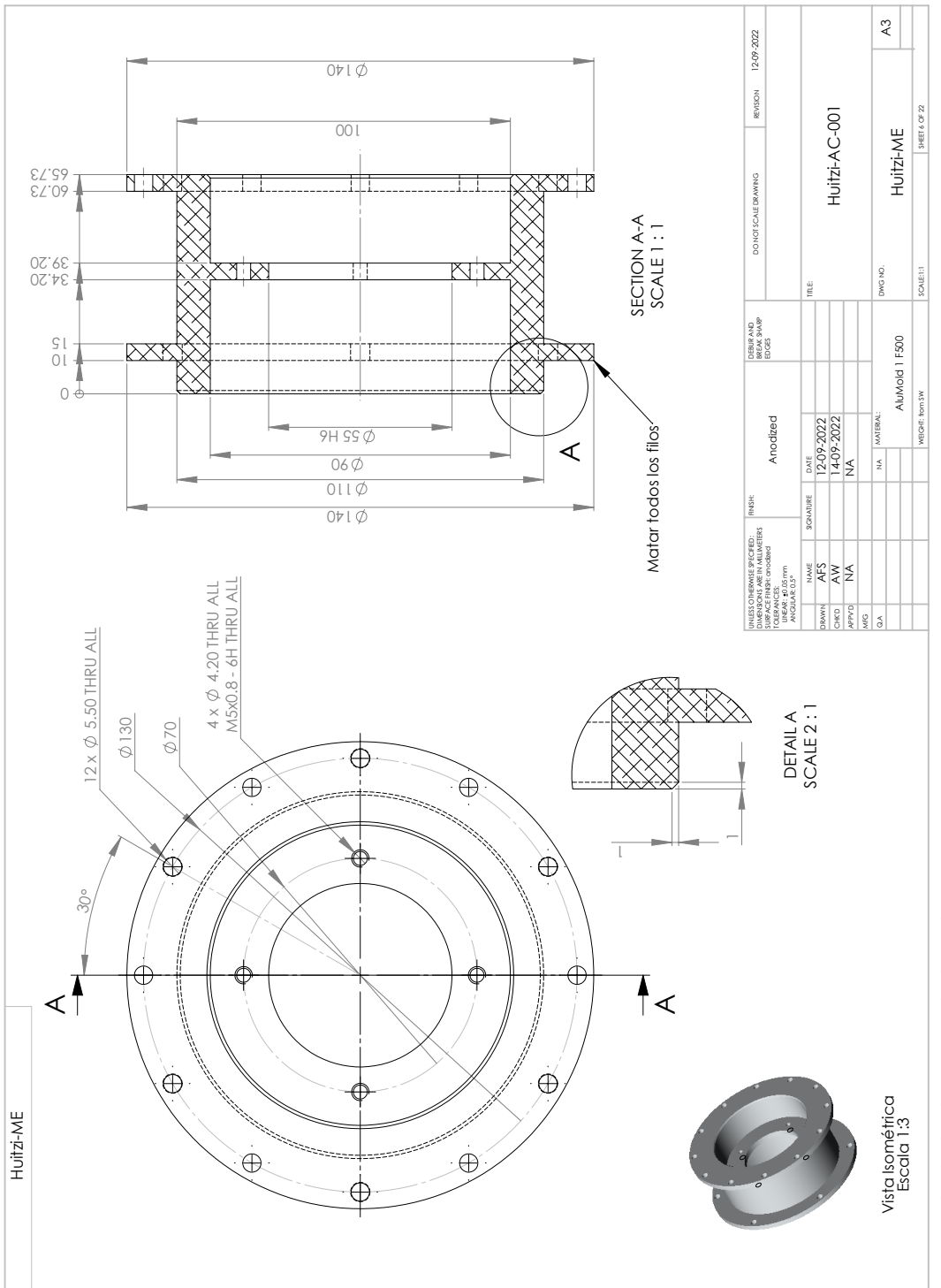


Figure 15.30: Drawing of part 2: the main barrel.

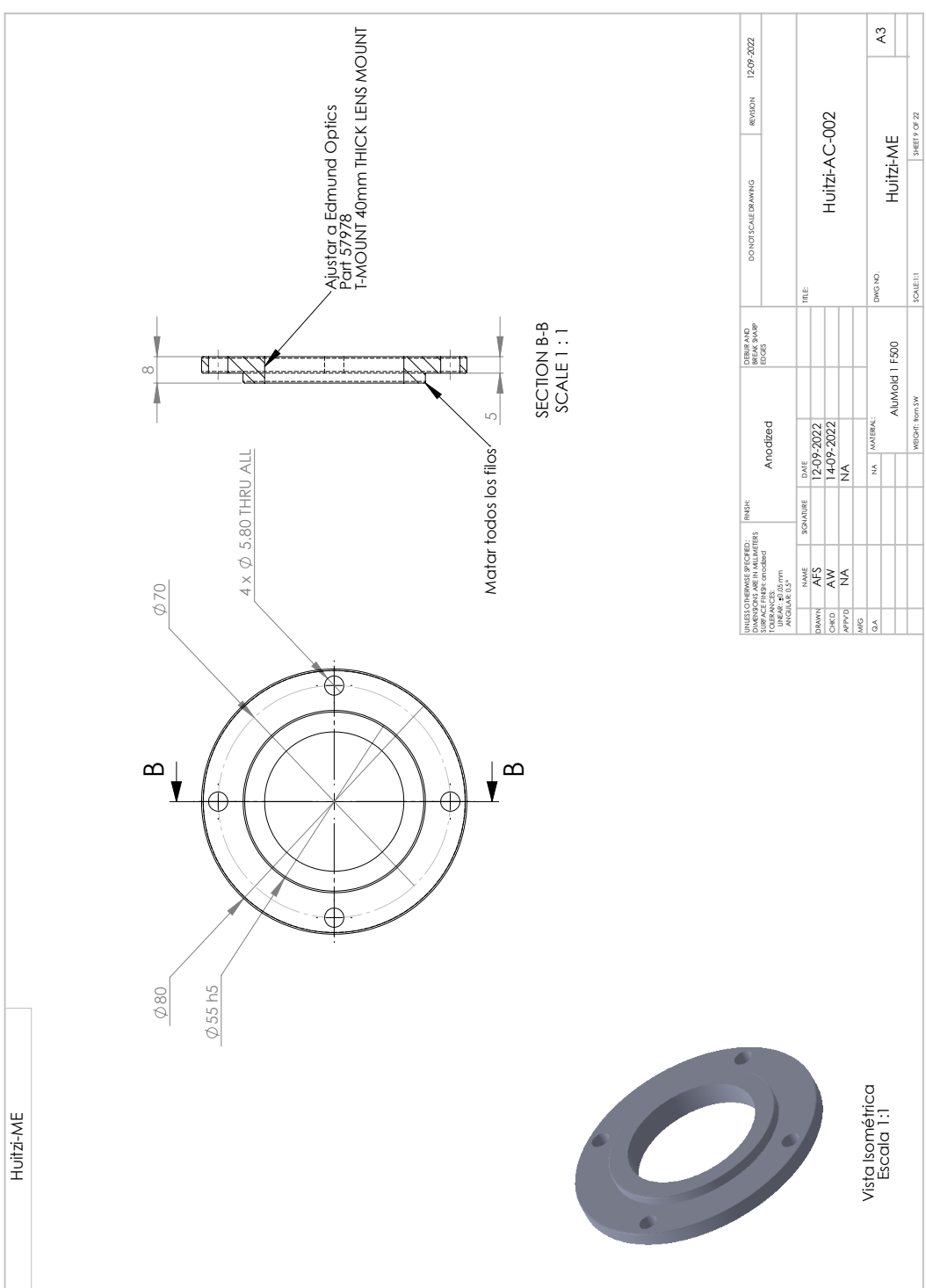


Figure 15.31: Drawing of part 3: the lens barrel ring.

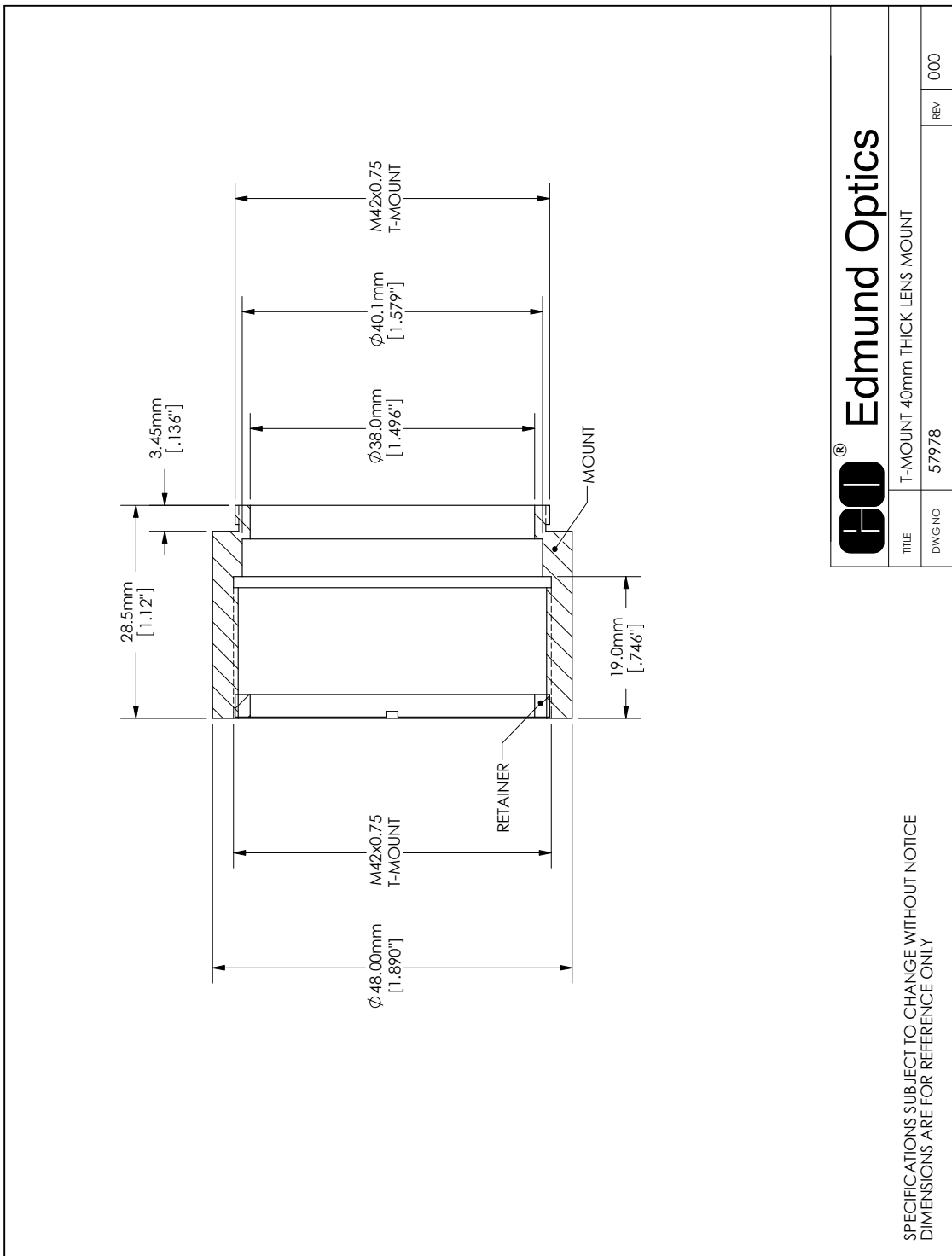


Figure 15.32: Drawing of part 4: the lens barrel.

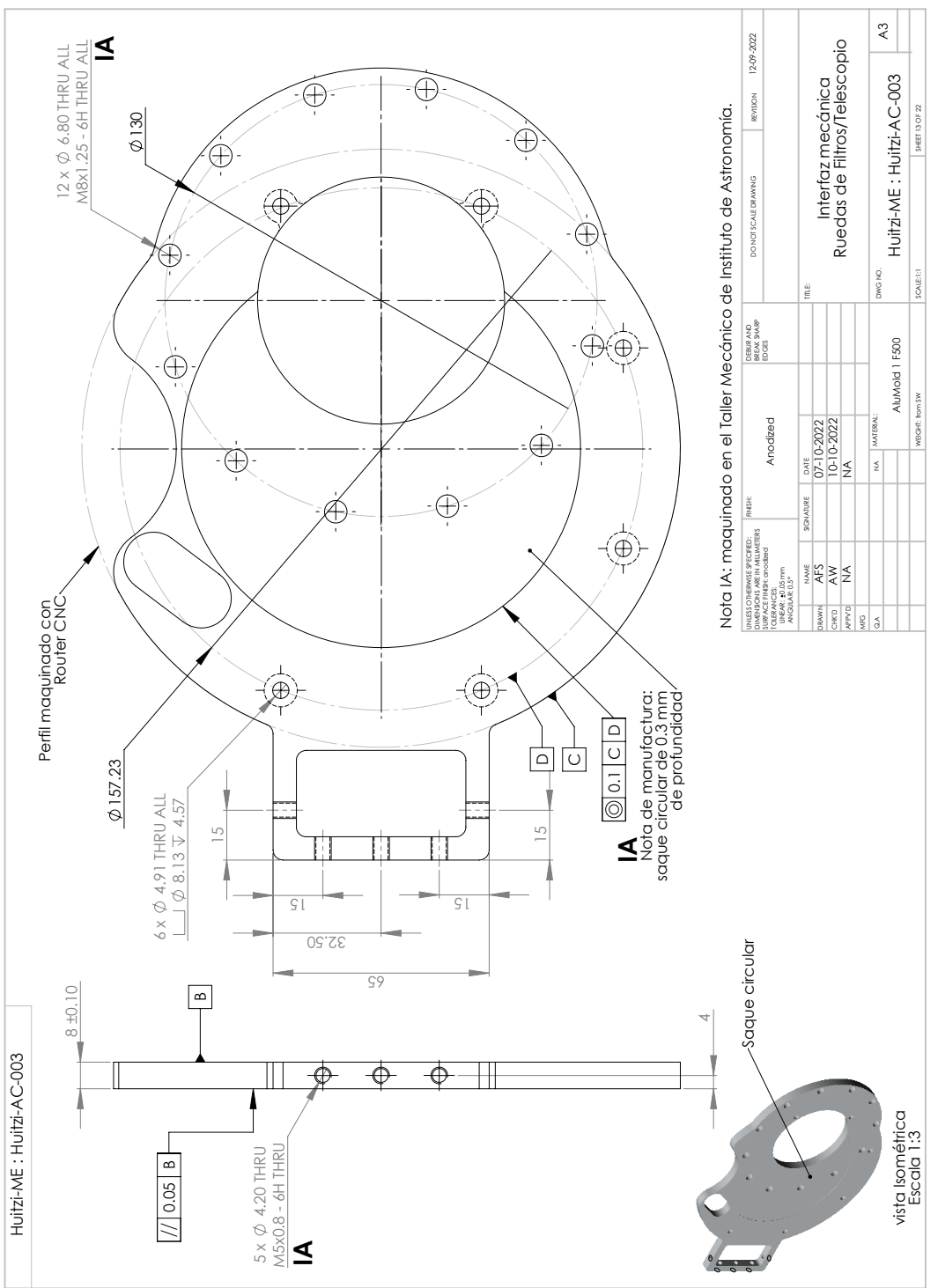


Figure 15.33: Drawing of part 5: the upper filter wheel interface plate.

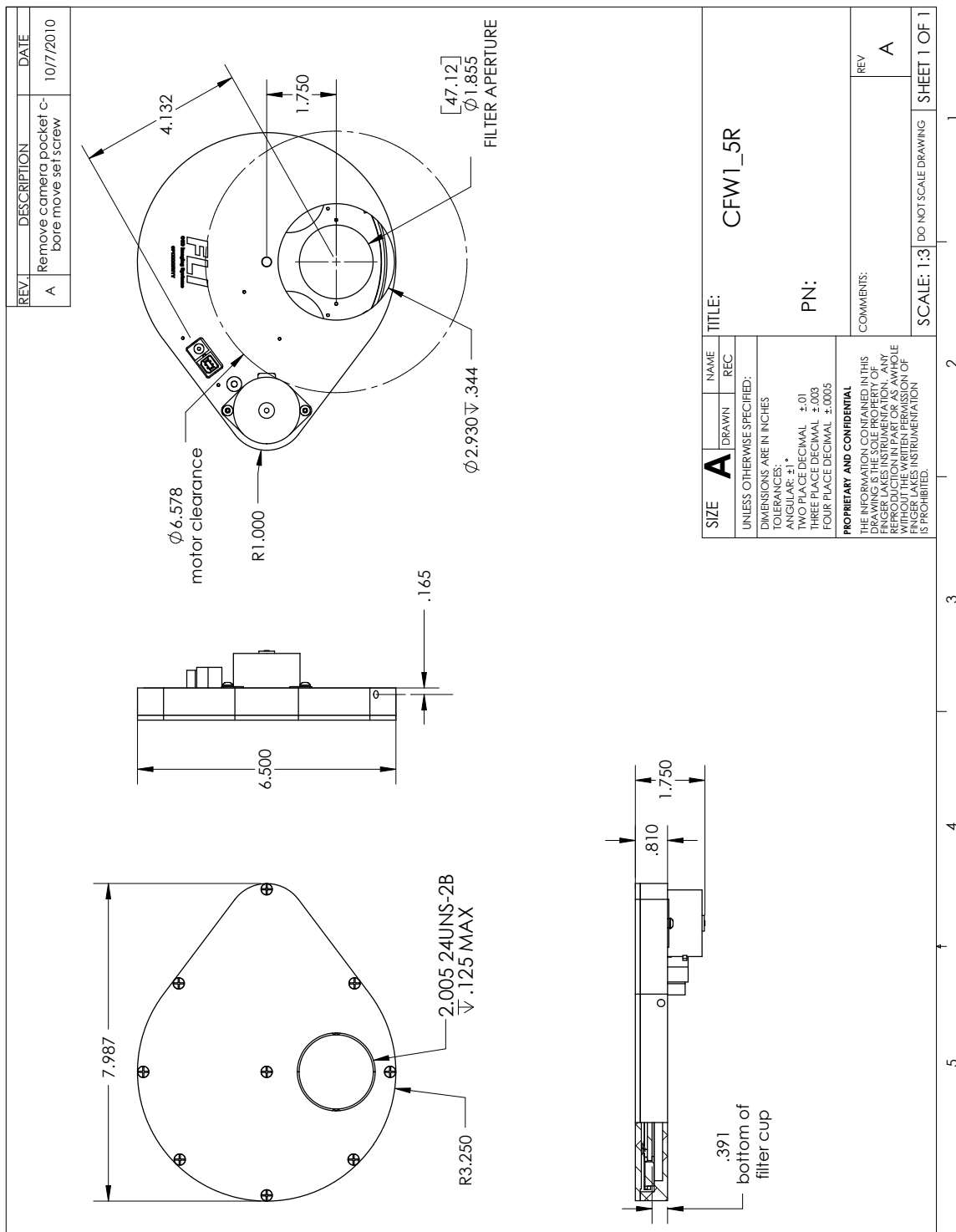


Figure 15.34: Drawing of part 6: the FLI CFW-1-5 filter wheel. The CFW-1-8 wheels differs only internally.

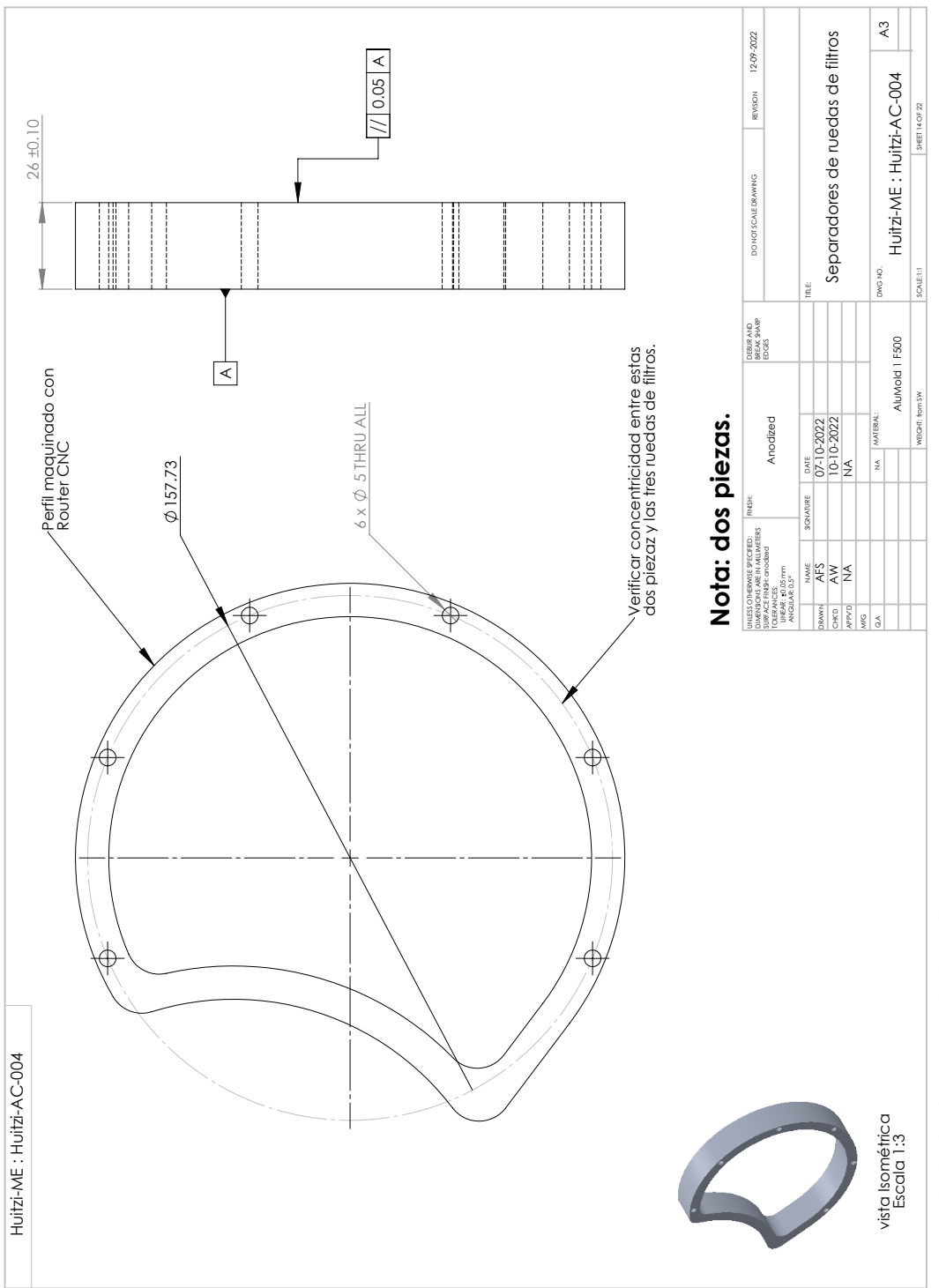


Figure 15.35: Drawing of part 7: the filter wheel separators.

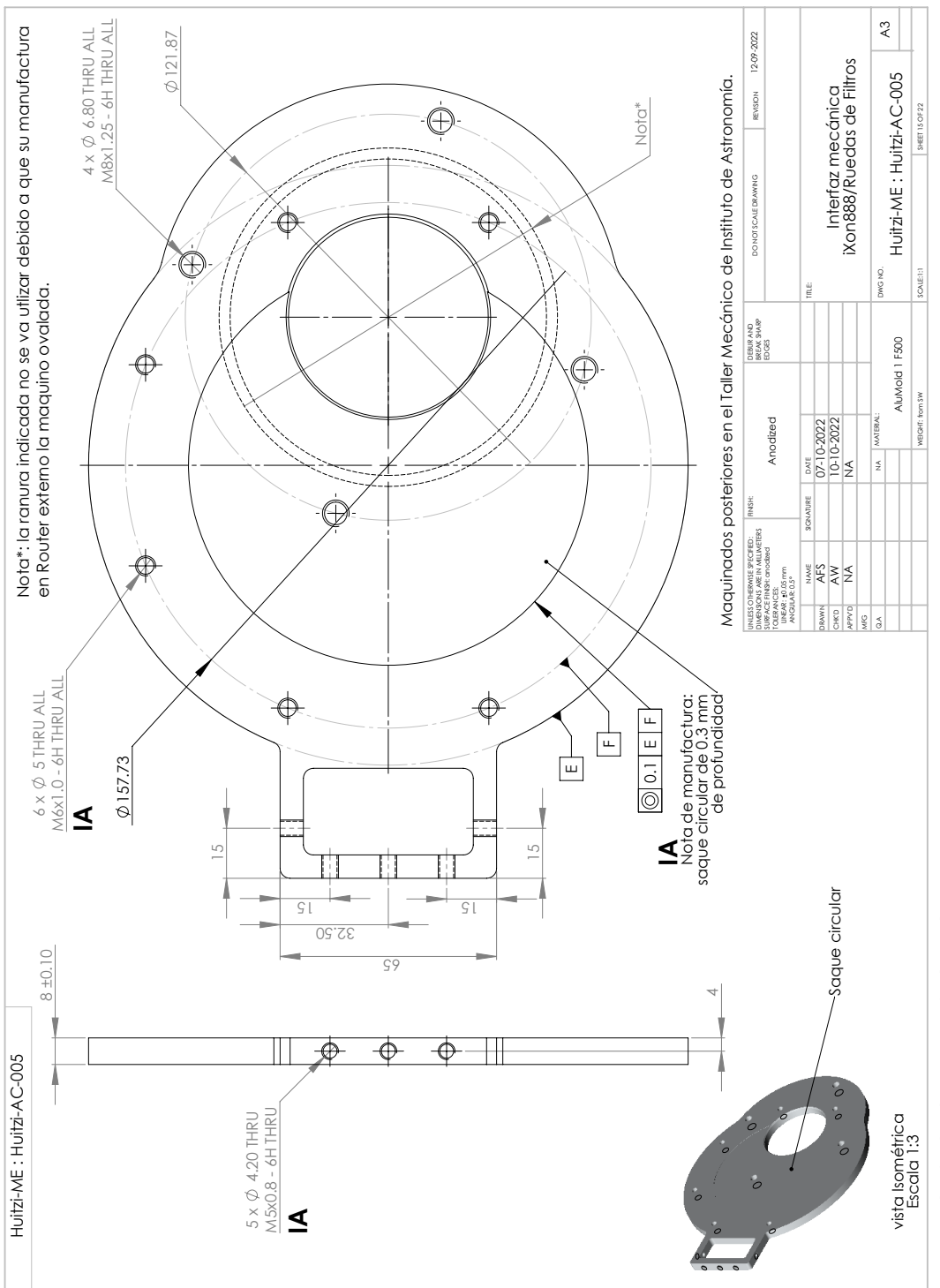


Figure 15.36: Drawing of part 8: the lower filter wheel interface plate.

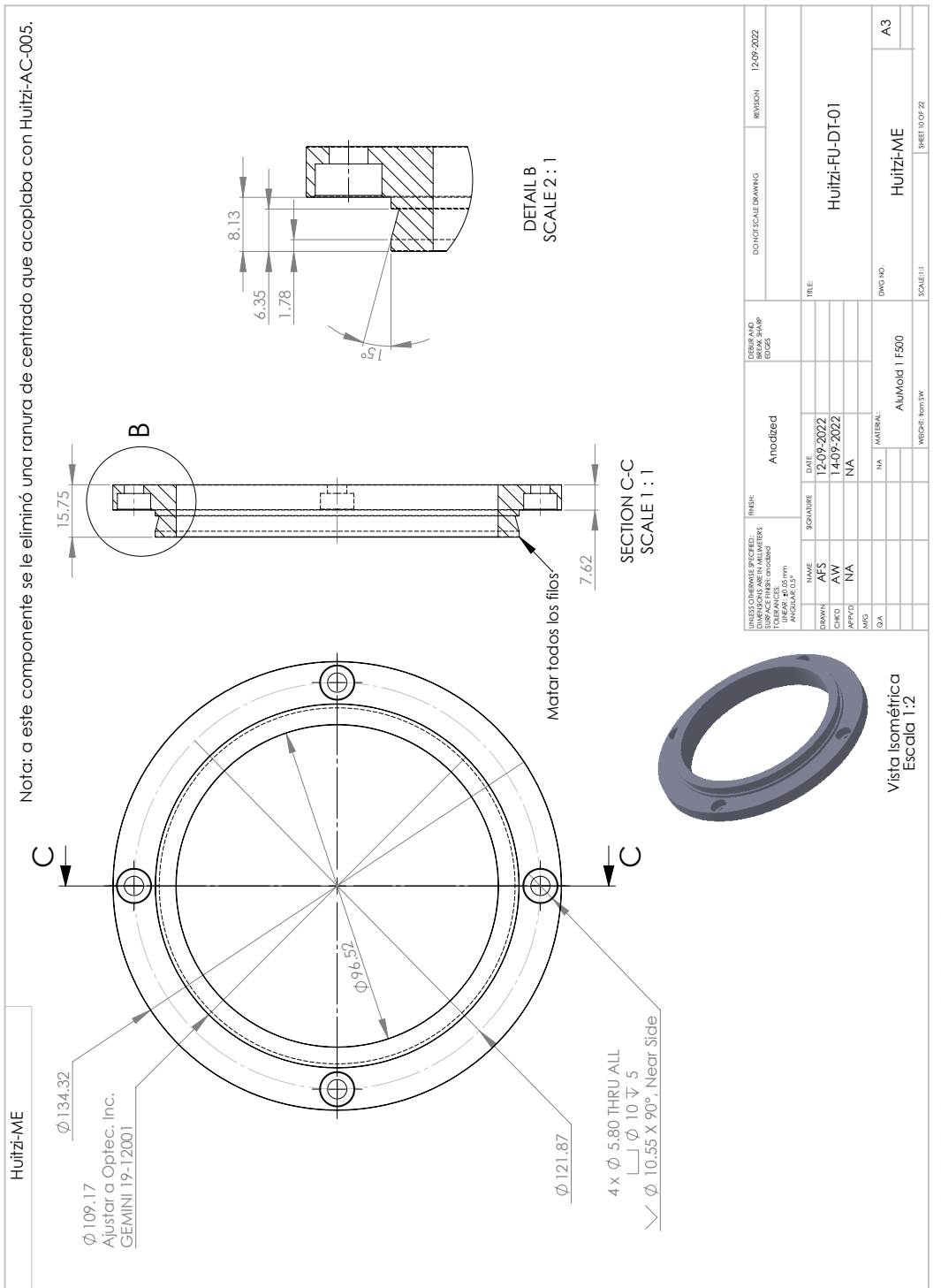


Figure 15.37: Drawing of part 9: the upper focuser interface ring.

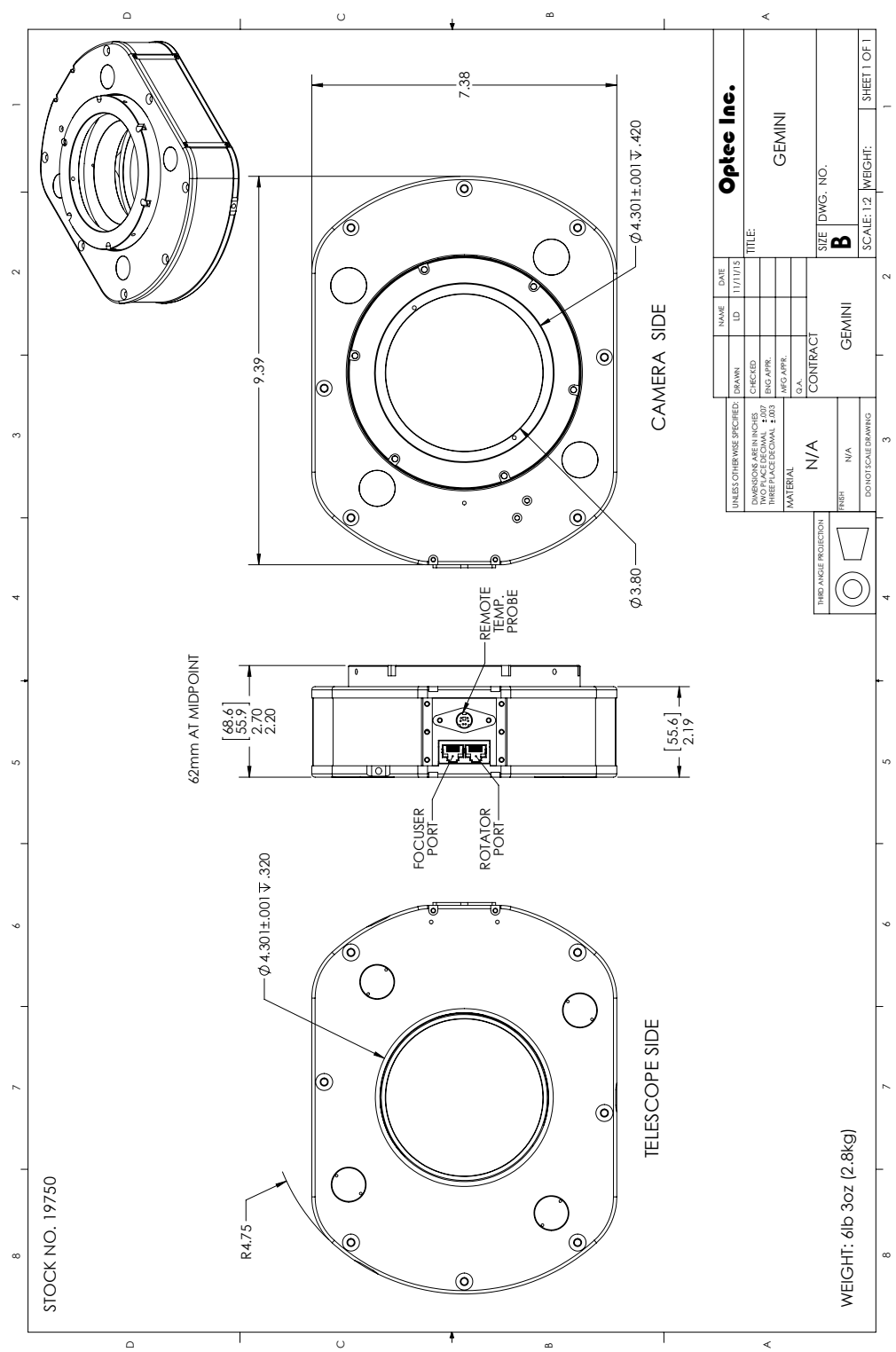


Figure 15.38: Drawing of part 10: the Optec Gemini focuser.

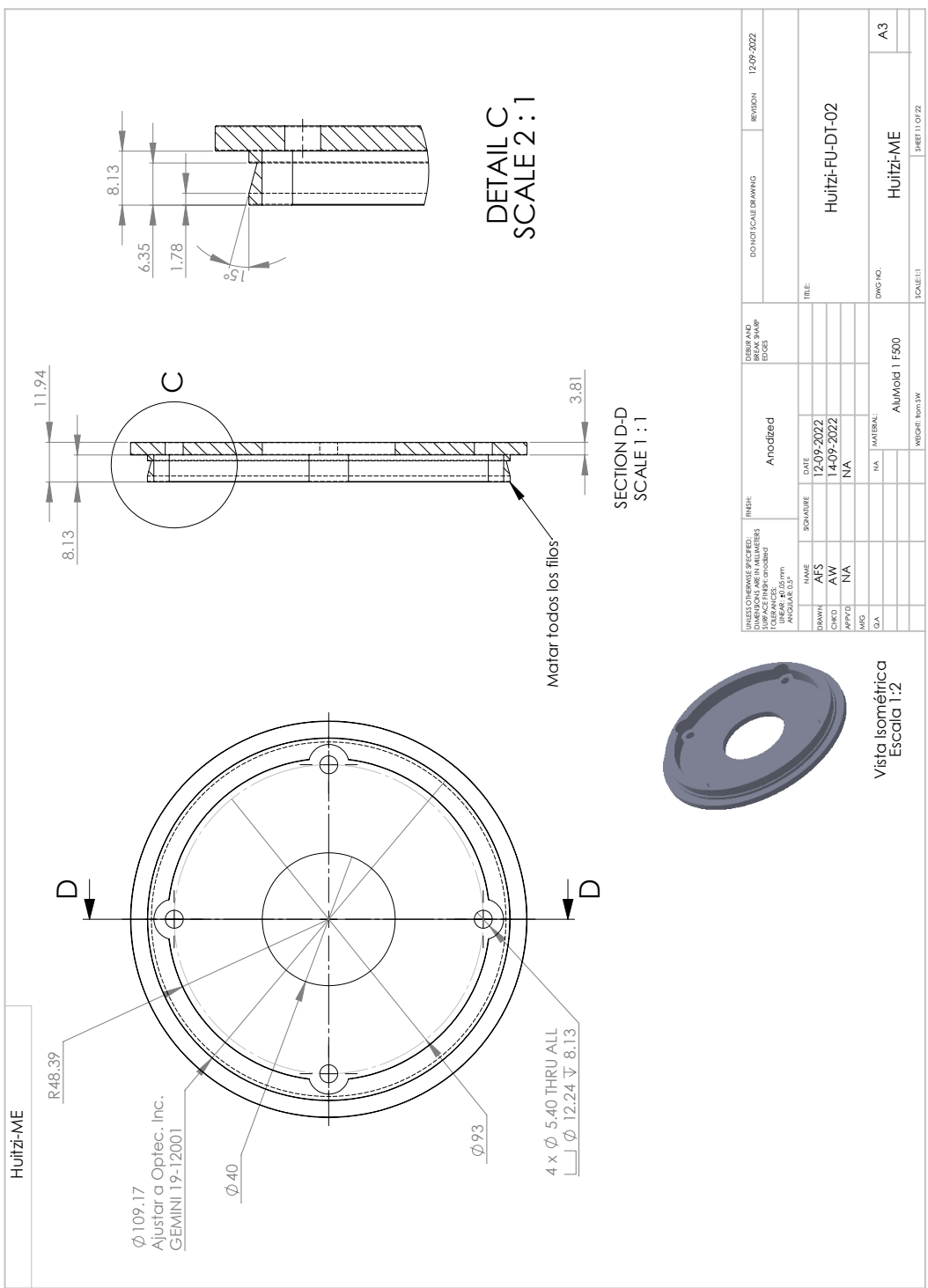


Figure 15.39: Drawing of part 11: the lower focuser interface ring.

## APPENDIX A: MECHANICAL DRAWINGS

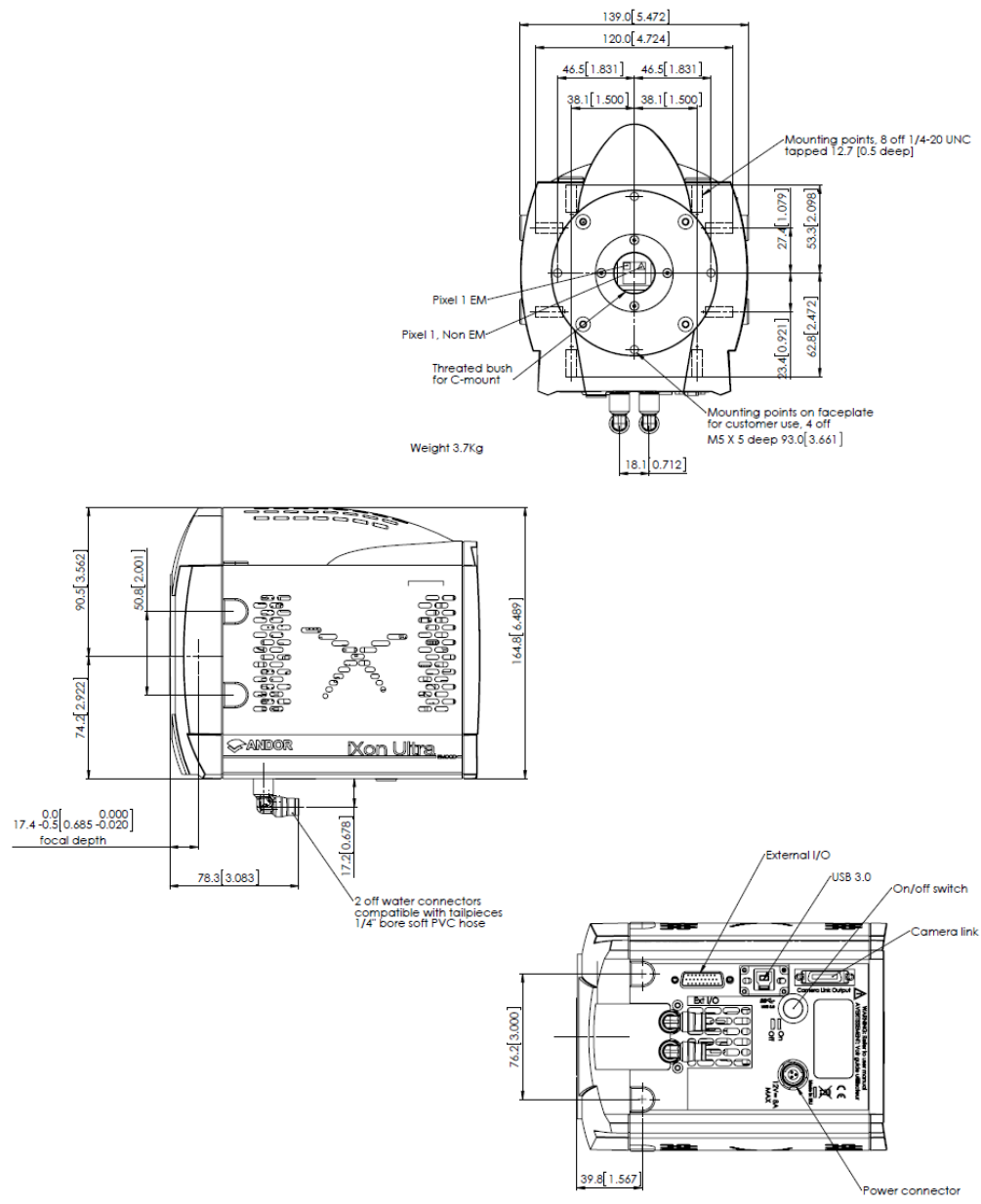


Figure 15.40: Drawing of part 12: the detector head.

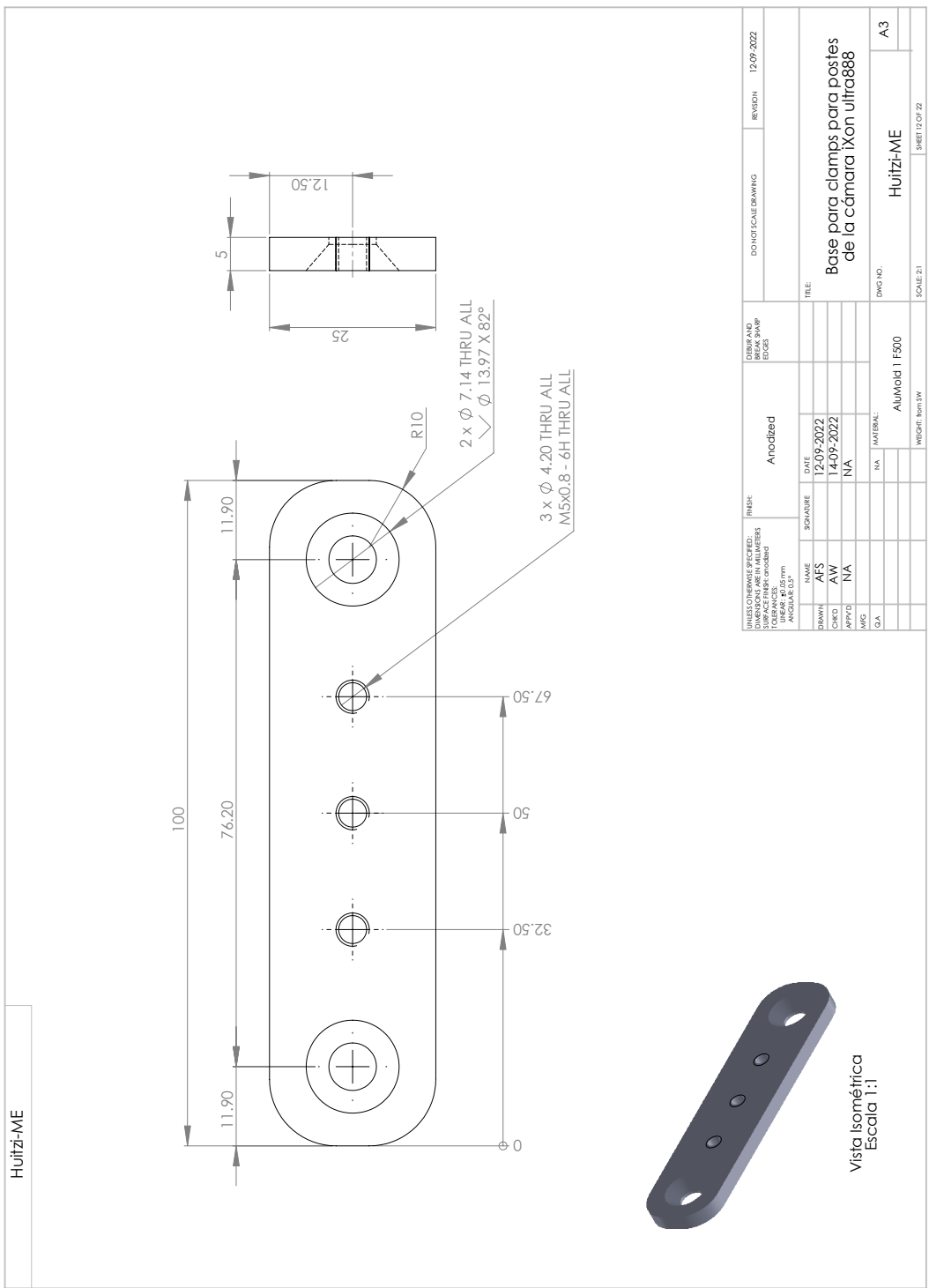


Figure 15.41: Drawing of part 14: the detector cable support plate.

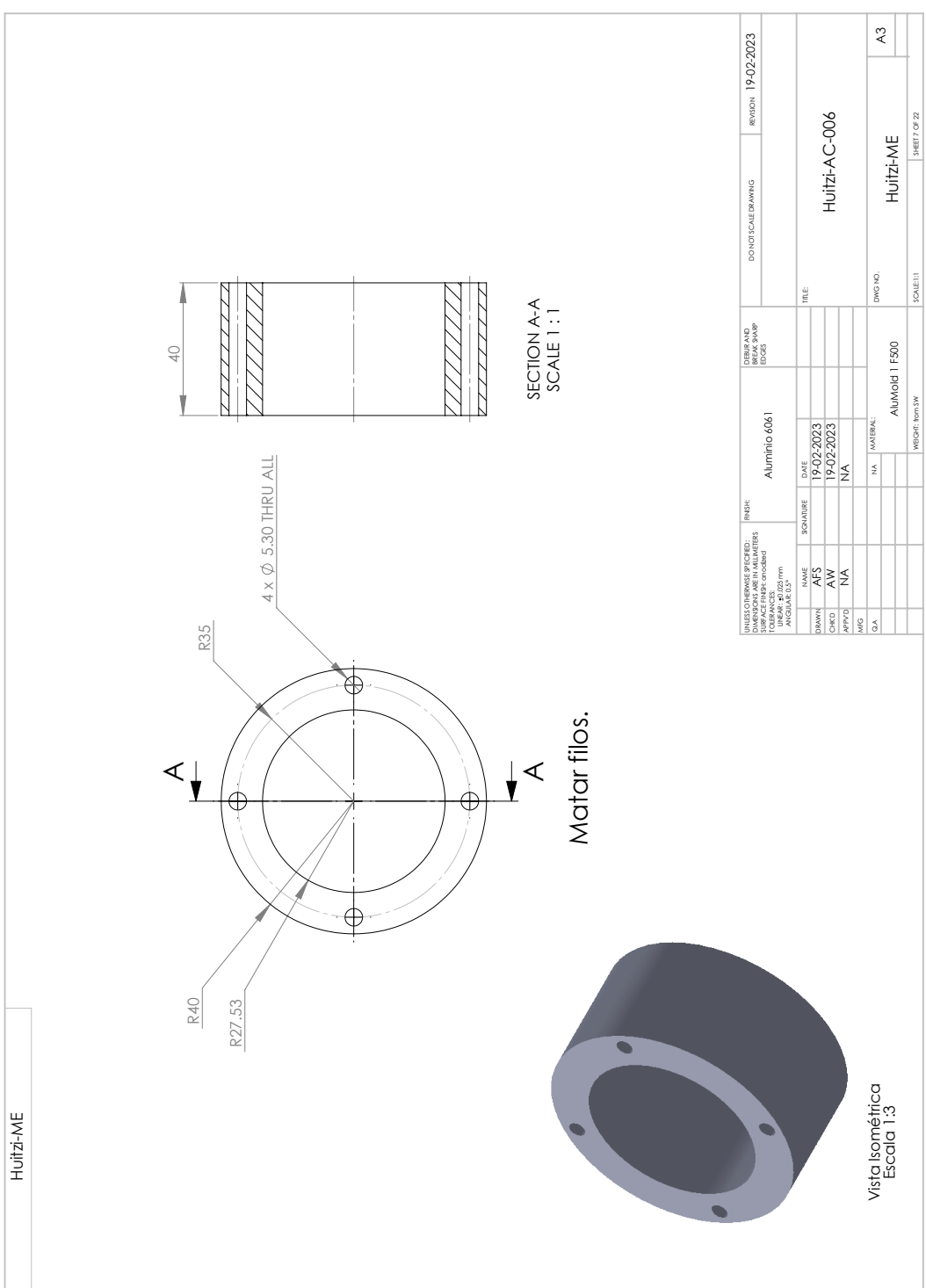


Figure 15.42: Drawing of part X: the lens barrel separator.

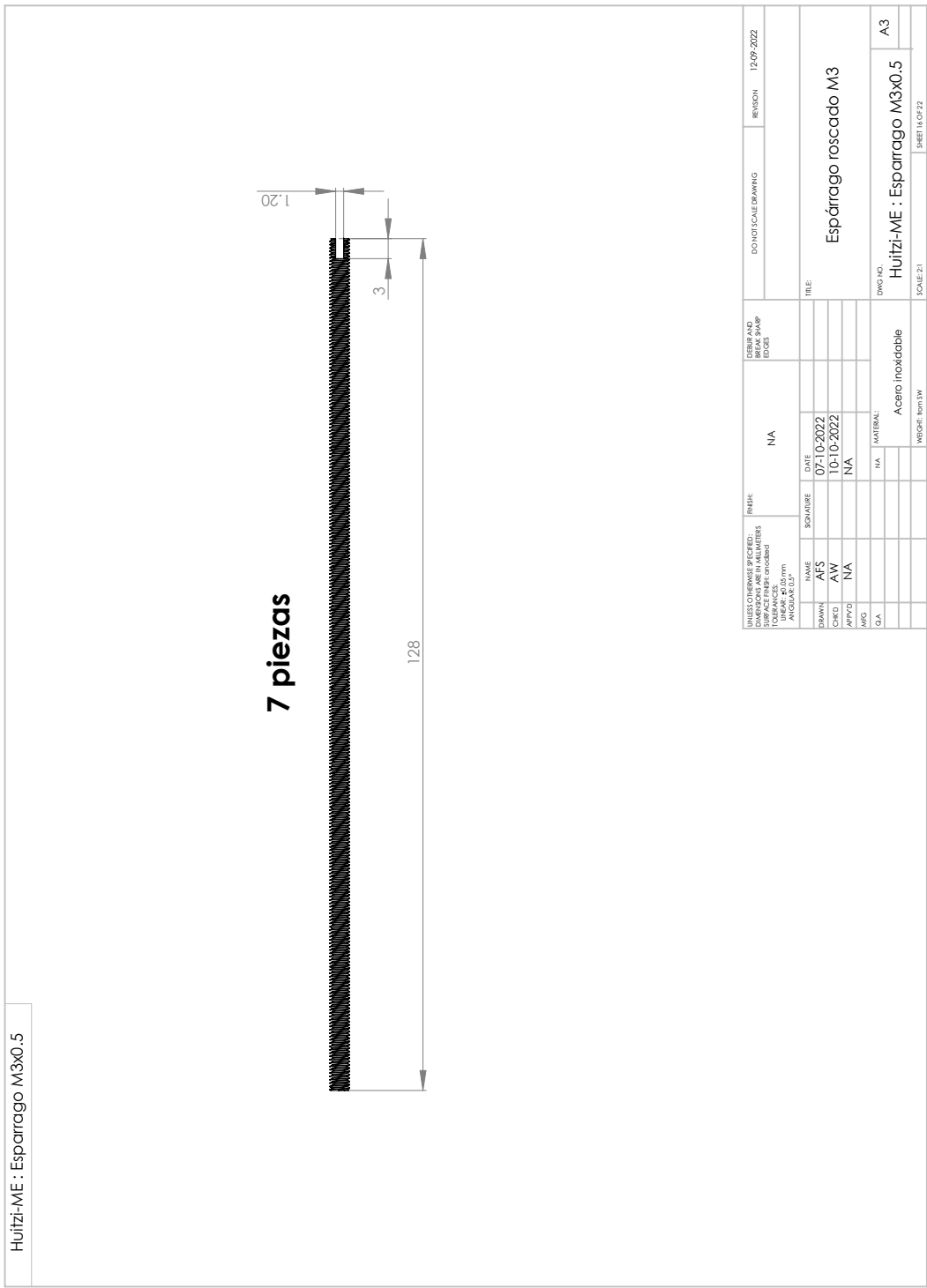


Figure 15.43: Drawing of part Y: the threaded rods.

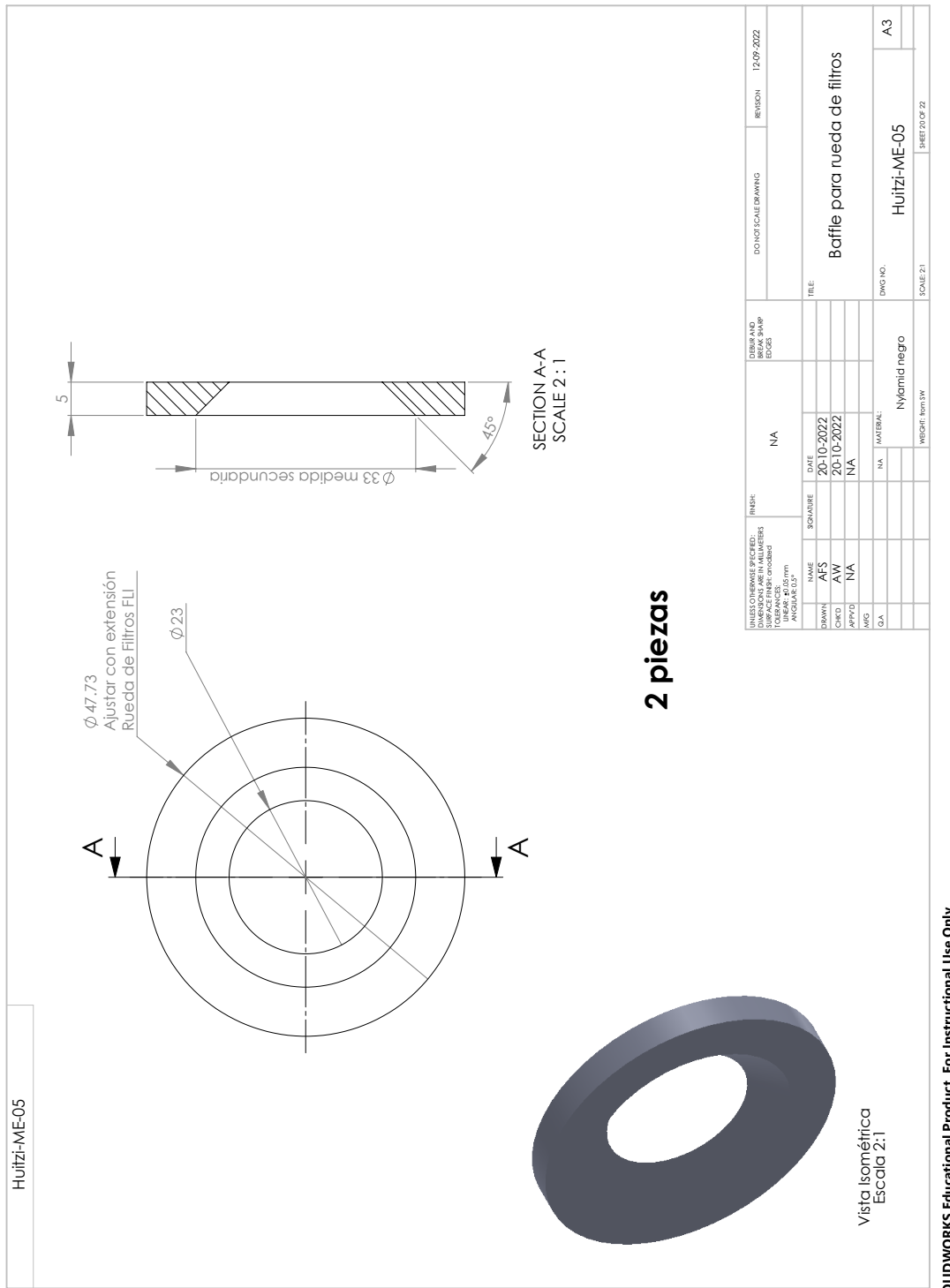


Figure 15.44: Drawing of part Z: the internal baffles.

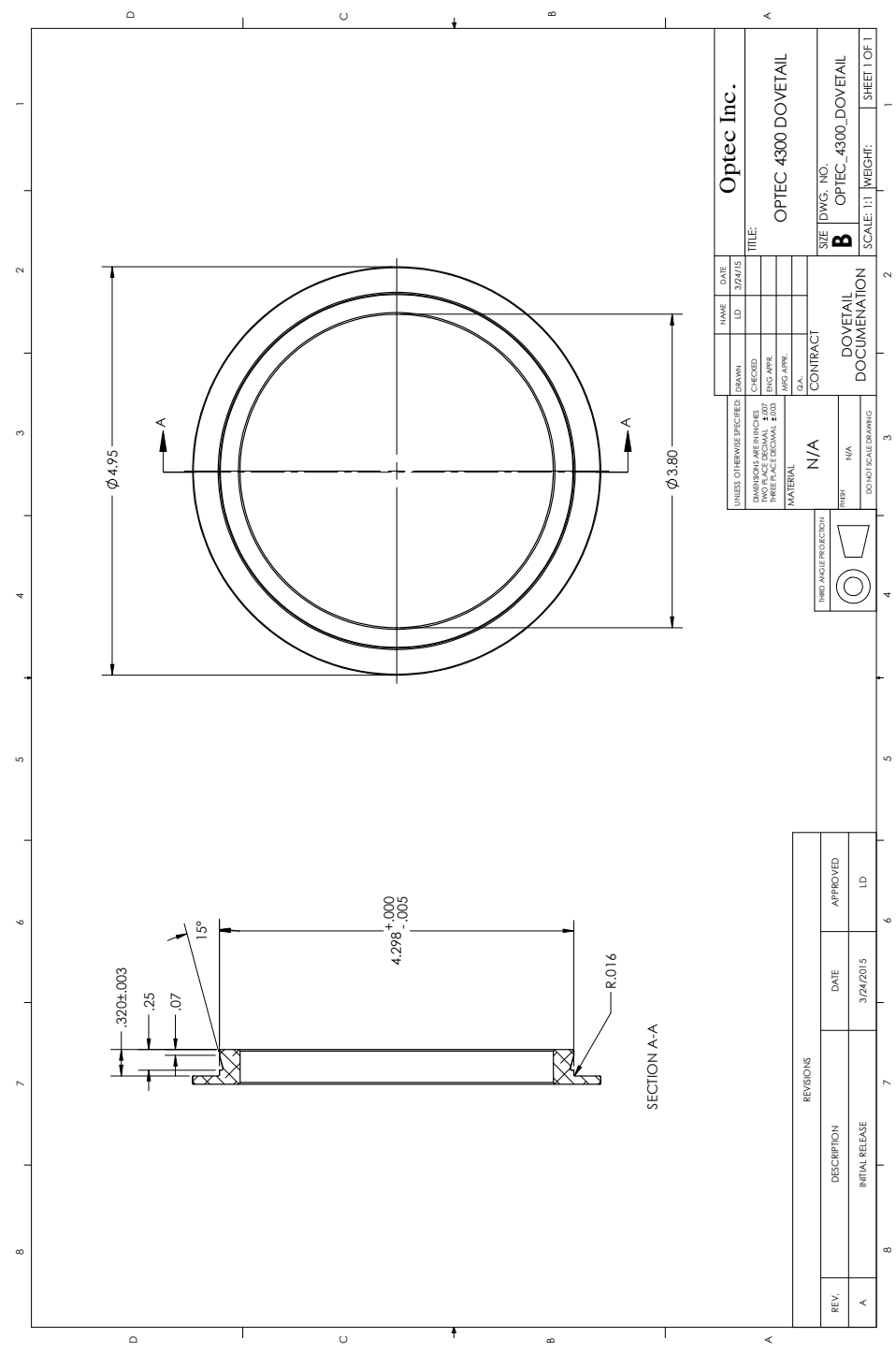


Figure 15.45: Drawing of part the Optec focuser dovetail rings. This is not part of the instrument, but serves as a specification for the dovetail on the two focuser interface plates.



Figure 15.46: The FLI-supplied adapters are installed on the lower sides of filter wheels A and B. Together with two examples of part Z, they act as internal baffles.

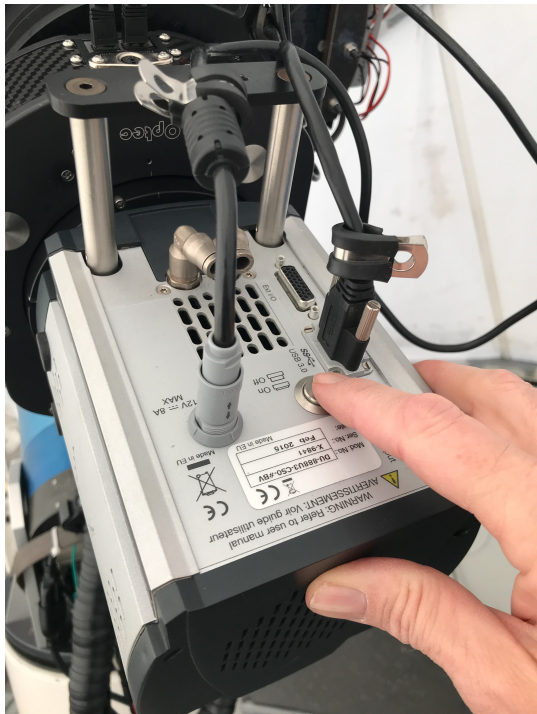


Figure 15.47: The detector head power switch.

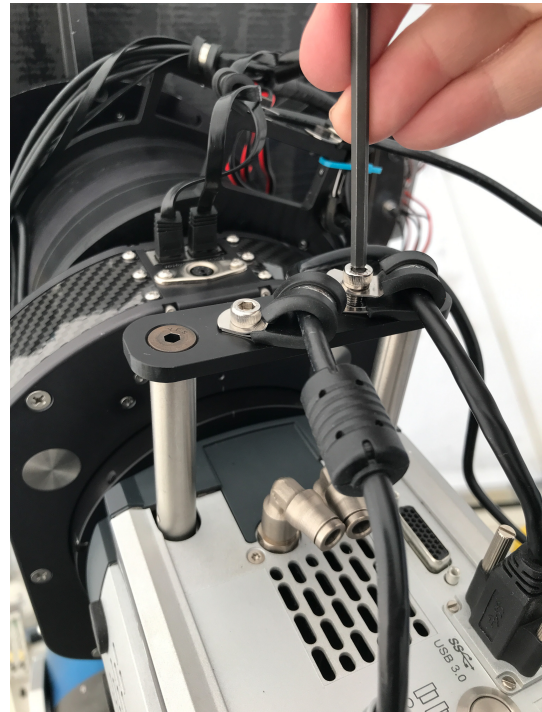


Figure 15.48: The detector head cable clamps.

## Procedure

1. Go to the shed. Put on harnesses and helmets. Move the enclosure switch to LOCAL. Open the enclosure to 60 degrees. Ascend to the platform.
2. Dismount the detector.
  - (a) Switch off the detector head by pressing the power switch. See Figure 15.47.
  - (b) With the 4 mm hex key, unfasten the detector head cable clamps. Then disconnect the detector power and USB cables. See Figures 15.48 and 15.49.
  - (c) One person should now support the detector head. The other person should use the 5/64-inch hex key to loosen the set screws between the detector head and the focuser that hold the lower dovetail. In each barrel there are two screws, a shorter, outer, flat-header screw that serves as a lock screw and a longer, inner, oval-headed screw that serves to make contact with the dovetail. Once these are loose, the detector head can be removed from the focuser. See Figure TODO.
  - (d) Place the detector head on a clean surface with the opening toward the detector downwards.
3. Dismount the focuser.
  - (a) Disconnect the focuser control cables. See Figure 15.50.



Figure 15.49: The detector head cables.



Figure 15.50: The focuser cables.

- (b) One person should now support the focuser. The other person should use the 5/64-inch hex key to loosen the set screws between the filter wheels and the focuser that hold the upper dovetail. In each barrel there are two screws, a shorter, outer, flat-header screw that serves as a lock screw and a longer, inner, oval-headed screw that serves to make contact with the dovetail. Once these are loose, the focuser can be removed. See Figure TODO.
  - (c) Place the focuser on a clean surface.
4. Dismount the filter wheel block.
- (a) Before disconnecting the filter wheel cables, take photos so that you can remember how to reconnect them.
  - (b) Each filter wheel has one power cable and one USB cable. These cables cannot be disconnected from the filter wheels without disassembling the whole block. Therefore, disconnect the USB cables from the USB hub on the telescope and, with the 2 mm flat-bladed screwdriver, disconnect the power cables from the power block on the telescope. Then use a 4 mm hex key to remove the clamps so that the cables are loose.
  - (c) One person should now support the filter wheel block. The other person should use the 8 mm wrench to loosen the twelve screws that hold the filter wheels to the main barrel. Once these are

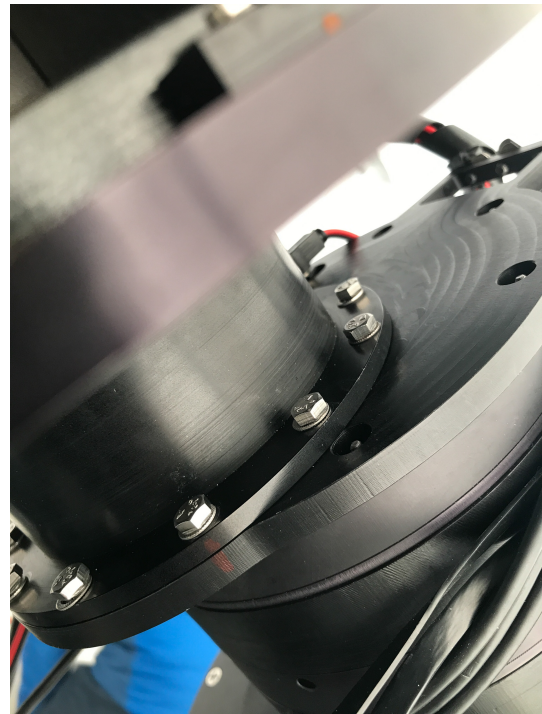


Figure 15.51: The filter wheel block screws. Note the alignment marks.

loose, the filter wheel block can be removed. See Figure 15.51.

- (d) Place the filter wheel block on a clean surface.

#### 5. Dismount the main barrel.

- (a) One person should now support the main barrel. The other person should use the 4 mm hex key to loosen the size screws that hold the main barrel to the instrument flange. Once these are loose, the main barrel can be removed. See Figure 15.52.
- (b) Place the filter wheel block on a clean surface.

## 15.8.2 Mounting the Instrument

### Requirements

You will need:

- Two persons.
- The key to the shed.
- 4 mm and 5/64-inch hex keys.
- 2 mm flat-bladed screwdriver.
- Cutting pliers and cable ties.
- 8 mm wrench



Figure 15.52: The main barrel screws. Note the alignment marks.

### Procedure

1. Go to the shed. Put on harnesses and helmets. Move the enclosure switch to LOCAL. Open the enclosure to 60 degrees. Ascend to the platform.

2. Mount the main barrel.

- (a) One person should insert the main barrel into the instrument flange and rotate it to align the alignment marks. The other person should use the 4 mm hex key to tighten the six screws that hold the main barrel to the instrument flange. See Figure 15.52.

3. Mount the filter wheel block.

- (a) One person should support the filter wheel block against the main barrel and rotate it to align the alignment marks. The other person should use the 8 mm wrench to tighten the twelve screws that hold the filter wheels to the main barrel. See Figure 15.51.

- (b) Connect the USB cables to the USB hub on the telescope and, with the 2 mm flat-bladed screwdriver, connect the power cables to the power block on the telescope. Then use a 4 mm hex key to fasten the clamps and tidy the cables (using cable ties where appropriate).

4. Mount the focuser.

- (a) One person should now support the focuser against the filter wheel block and rotate it so that the control cable sockets are away from the mount. The other person should use the 5/64-inch hex key to tighten the set screws between the filter wheels and the focuser that hold the upper dovetail. In each barrel there are two screws, a shorter, outer, flat-header screw that serves as a lock screw and a longer, inner, oval-headed screw that serves to make contact with the dovetail. See Figure TODO.

- (b) Connect the focuser control cables. See Figure 15.50.

5. Mount the detector.

- (a) One person should now support the detector head against the focuser and rotate it so that the control cable sockets are away from the mount. The other person should use the 5/64-inch hex key to tighten the set screws between the detector head and the focuser that hold the lower dovetail. In each barrel there are two screws, a shorter, outer, flat-header screw that serves as a lock screw and a longer, inner, oval-headed screw that serves to make contact with the dovetail. See Figure TODO.

- (b) With the 4 mm hex key, fasten the detector head cable clamps. Then connect the detector power and USB cables. See Figures 15.48 and 15.49.

- (c) Switch on the detector head by pressing the power switch. See Figure 15.47.

### 15.8.3 Disassembling the Filter Wheel Block

#### Requirements

You will need:

- Two persons.
- The key to the shed.
- 2 mm flat-bladed screwdriver.
- Phillips screwdriver.
- 4 mm hex key
- 6 mm hex socket

#### Procedure

1. Go to the shed. Put on harnesses and helmets. Move the enclosure switch to LOCAL. Open the enclosure to 60 degrees. Ascend to the platform.
2. Dismount the instrument, including filter wheel block. See § 15.8.1.

3. Place the filter wheel block in a clean plastic bag. Then carefully transport it from the platform to a clean place.
4. Remove the upper focuser interface ring from the lower filter wheel interface plate.  
Use the 4 mm hex key to remove the four M5 screws that hold the ring in place. See Figure TODO.
5. The filter block is held together by six M3 threaded rods. The lower ends of the rods are threaded into inserts in the lower filter wheel plate and are slotted to accept a flat-bladed screwdriver. The upper ends are fixed by nuts. Place a flat-bladed screwdriver in the lower slot. Support the screwdriver so that the rod does not turn. Use a 6 mm hex socket to remove the nuts.
6. Once all of the nuts have been removed, the filter block can be disassembled piece-by-piece from the top.
7. The filter wheels can be disassembled by removing the nine Phillips screws that hold their cover to their body.

#### 15.8.4 Assembling the Filter Wheel Block

##### Requirements

You will need:

- 2 mm flat-bladed screwdriver.
- Phillips screwdriver.
- 4 mm hex key
- 6 mm hex socket

##### Procedure

1. The filter wheels can be assembled by tightening the nine Phillips screws that hold their cover to their body. Do not over-tighten the central one, as this can cause the wheel to jam.
2. Assemble the filter block piece-by-piece from the bottom. See Figure 15.28.
3. The filter block is held together by six M3 threaded rods. The lower ends of the rods are threaded into inserts in the lower filter wheel plate and are slotted to accept a flat-bladed screwdriver. The upper ends are fixed by nuts. Place a flat-bladed screwdriver in the lower slot. Support the screwdriver so that the rod does not turn. Use a 6 mm hex socket to tighten the nuts.
4. Fasten the upper focuser interface ring to the lower filter wheel interface plate.  
Use the 4 mm hex key to tighten the four M5 screws that hold the ring in place. See Figure TODO.
5. Place the filter wheel block in a clean plastic bag. Then carefully transport it to the platform.

## 15.9 Bibliography

- “Andor iXon Ultra 888 Data Sheet”, Andor, May 2014.
- “Andor iXon Ultra & Life 888 Hardware Guide”, Andor, Version 1.8 of 30 September 2019.
- Bessell, M.S., 1990, PASP, 102, 1181: “UBVRI Passbands”.
- Bessell, M., & Murphy, S., 2012, PASP, 124, 140: “Spectrophotometric Libraries, Revised Photonic Passbands, and Zero Points for UBVR<sub>I</sub>, Hipparcos, and Tycho Photometry”.
- “CCD201-20 Datasheet”, Teledyne e2v, Version 7 of August 2019.
- Cousins, A.W.J., 1976, MNRAS, 81, 25: “VRI standards in the E regions”.
- Oke, J.B., & Gunn, J.E., 1983, ApJ, 266, 713: “Secondary Standard Stars for Absolute Spectrophotometry”

# **Part IV**

# **Control System**

## **Part V**

# **Obsolete Components**